

© Copyright 2019

Dylan S. Reinsdorf

Development of a Robotic Unloader Brace for Investigation of Conservative Treatment of
Medial Knee Osteoarthritis

Dylan S. Reinsdorf

A thesis

submitted in partial fulfillment of the
requirements for the degree of

Master of Science in Mechanical Engineering

University of Washington

2019

Committee:

Patrick Aubin, Chair

Katherine Steele

Sawyer Fuller

Program Authorized to Offer Degree:

Mechanical Engineering

University of Washington

Abstract

Development of a Robotic Unloader Brace for Investigation of Conservative Treatment of Medial Knee Osteoarthritis

Dylan S. Reinsdorf

Chair of the Supervisory Committee:

Patrick Aubin, Ph.D.

Affiliate Assistant Professor

Mechanical Engineering

Knee osteoarthritis (KOA) is a painful and debilitating condition that is associated with mechanical loading of the knee joint. Numerous conservative treatment strategies have been developed to decrease pain, improve mobility, and delay time to total joint replacement. Unloader braces are commonly prescribed for medial uni-compartmental KOA, however their evidence of efficacy is inconclusive and limited by user compliance. Typical commercial braces transfer load from the medial compartment to the lateral knee compartment by applying a continuous brace abduction moment (BAM). We propose that brace utilization and effectiveness could be improved with a robotic device that intelligently modulates BAM in real time over the course of a step, day, and year to better protect the knee joint, improve pain relief, and increase comfort. To this end, we

developed a robotic unloader knee brace ABLE (active brace for laboratory exploration) to flexibly emulate and explore different active and passive brace behaviors that may be more efficacious than traditional braces. The system is capable of modulating BAM within each step per researcher defined unloading profiles. ABLE was realized as a lightweight orthosis driven by an off-board system containing a servo motor, drive, and real-time controller. Frequency response and intra-step trajectory tracking during level-ground walking were evaluated in a single healthy human subject test to verify system performance. The system tracked trajectories with a root mean square error of 0.18 to 0.58 Nm for conditions varying in walking speed, 85-115% nominal, and trajectory peak BAM, 2.7 to 8.1 Nm. Biomechanical and subjective outcomes will be evaluated next for KOA patients to investigate how novel robotic brace operation affects pain relief, comfort, and KOA progression.

TABLE OF CONTENTS

List of Figures	3
List of Tables	6
List of Abbreviations	7
Chapter 1. Introduction	9
1.1 <i>Knee Osteoarthritis Background</i>	9
1.2 <i>Knee Loading</i>	9
1.3 <i>Medial Unloader Braces</i>	10
1.4 <i>Powered Assistive Devices</i>	11
1.5 <i>Purpose</i>	12
Chapter 2. System Development.....	14
2.1 <i>System Definition</i>	14
2.2 <i>Knee Brace Design</i>	15
2.3 <i>Off-board System Overview</i>	17
2.4 <i>Motor selection</i>	18
2.5 <i>Motor transmission design</i>	21
2.6 <i>Drive power circuit design</i>	24
Chapter 3. Software and Control Law Development.....	25
3.1 <i>Trajectory Generation</i>	26
3.2 <i>Percent Gait Cycle Estimation</i>	28

3.3	<i>Compensation</i>	30
Chapter 4.	Methods: Human Subject Testing	34
4.1	<i>Bandwidth Performance Evaluation</i>	35
4.2	<i>Peak BAM Performance Evaluation</i>	37
4.3	<i>Key Question Evaluation</i>	37
Chapter 5.	Results	39
5.1	<i>Bandwidth Performance Evaluation</i>	39
5.2	<i>Peak BAM Performance Evaluation</i>	40
5.3	<i>Key Question Evaluation</i>	41
Chapter 6.	Discussion and conclusion	44
6.1	<i>Bandwidth Performance Evaluation</i>	44
6.2	<i>Key Question Evaluation</i>	44
6.3	<i>Conclusion</i>	46
Bibliography	48
Appendix A:	Code and Results for Off-board System Motor Specification	51
Appendix B:	Motor Transmission Analysis and Design	58
Appendix C:	Motor Drive Power Circuit Design	73
Appendix D:	Code and Example Result for Trajectory Generation	82

LIST OF FIGURES

- Figure 1. Common medial unloader brace design with three-point bending principle. Strut bending (shown in the ‘Load’ state) generates an abduction moment. The strut is bent when the applied force at the lateral condyle pad is reacted by strap grounding interfaces on the femur and tibia. Load is applied when the condyle pad is translated toward the knee in the medial direction. The loading states and generated BAM are depicted with the classical mechanical embodiment of simply supported beam with central load. Maximum BAM is reached at location ‘b’, the lateral condyle pad. 10
- Figure 2. Pneumatic unloader brace with soft structure studied in [17]. Arrows point to air bladder locations used to generate BAM when inflated. Figure is copied from [17].12
- Figure 3. Unmodified OTS brace, Ottobock *Agilum Reactive*. BAM is generated via rotation of a screw which increases the valgus angle between the thigh and shank sections. This functionality is modified in the developed knee brace. 16
- Figure 4. Knee brace design, shown as the developed knee brace (right) and section view of the unloader mechanism 3D model (left). Tendon motion relative to the sheath generates an equal and opposite knee brace force F_{kb} at the condyle pad which contacts the medial side of the knee. The 3D printed leg model was used for control law and safety system development to prepare for human subjects testing..... 17
- Figure 5. Off-board system construction, host PC not shown. Although the host PC is required per the developed program architecture, its performance does not impact real-time control tasks..... 18
- Figure 6. Motor torque-speed trajectory for the input BAM versus percent gait cycle trajectory. 20
- Figure 7. Motor transmission. Bowden cable sheath (not shown) terminates at the ‘Bowden termination plate’, and cable tendon is wrapped around the sheave..... 21
- Figure 8. D-profile shaft cross section parameterization. Image copied from [24]..... 22
- Figure 9. Safety margins for shaft sizing analysis based on combined principle stress from bending and torsion..... 23

Figure 10. Motor drive power circuit (right) in rack-mountable enclosure and remote (left). The direct current power supply unit (DC PSU) powers the logic circuit which controls high level motor commands such as emergency stop, system on/off, etc. Both the remote and drive circuit are custom components. 24

Figure 11. ABLE software architecture. The host PC is used to interact with the system and perform non time critical tasks like data logging, the real-time controller performs time critical computation such as sensor input/output and motor control inputs (velocities), and the motor drive runs its own control law for tracking the desired motor velocities. The architecture was implemented in LabVIEW 2018. 25

Figure 12. Simplified control law design and distributed system implementation. Following initial trajectory X_T generation, the current %GC is estimated and reference BAM values passed to each compensator path: the desired BAM change $d\tau_d$ and desired BAM τ_d to the feedforward and feedback compensators, respectively. The feedforward control input V_{FF} is computed as the product of desired BAM change and feedforward gain K_{FF} . The feedback control input V_{FB} is computed from the error e between desired BAM and knee brace BAM τ_{kb} using a proportional-integral compensator PI. The motor drive, running a cascaded proportional-integral-derivative loop (shown in a simplified feedback form), tracks input desired velocity V_d from encoder measurement V_e and outputs motor velocity V_m . Sensor calibration constants are modeled as gains K_e , K_{kb} , and K_{gr} , for the motor encoder, knee brace load cell, and treadmill ground reaction force plate, respectively. 26

Figure 13. Example computed BAM trajectory with 0-15% gait cycle rise to 8 Nm peak BAM and 60 to 75% fall to 1 Nm minimum BAM. The average KAM is shown for a 100 kg healthy adult during level ground treadmill walking [15]. BAM is intended to reduce the KAM acting on the internal medial compartment, where BAM and KAM act in opposite directions: BAM in abduction, and KAM in adduction. 27

Figure 14. Gait cycle estimation algorithm design. The iterate index k refers to the current loop iteration and $k - 1$ to the previous. At each loop iteration, the time elapsed since the previous loop cycle, Δtk , is input from the CPU clock, and vertical GRF, Fz, k , from the instrumented treadmill force plate of the braced leg. Vertical GRF is thresholded and compared to the previous state to find rising edges in the signal and thus whether heel strike has occurred - the output is a binary bit bre, k . The diamond shaped block performs a

flagging operation and acts as a gate, switching between two paths $bre, k = 0$ for no rising edge/heel strike event and $bre, k = 1$ for the occurrence of a rising edge event. The flagging operation filters for false heel strike events by evaluating Equation 7. If no rising edge is detected ($bre, k = 0$, most loop iterations), then the routine bypasses the update layer, computes percent gait cycle Xgc, k , and finds the desired BAM τd from the trajectory, a transfer function from Xgc, k to τd . When rising edges are detected, the current time duration tk is passed to the Kalman Filter to update the gait cycle mean μgc and standard deviation σgc estimates, and tk is reset to zero before computing Xgc, k . 28

Figure 15. Motor torque inputs to BAM output for n=3 trials. The initial point for all trials is the minimum BAM value at 0 Nm motor torque, i.e. the lower of segment of each trial corresponds to increases in motor torque..... 31

Figure 16. Motor position inputs to BAM output for n=3 trials. The lower segment of each trial corresponds to increases in motor position, while the upper segment corresponds to decreases. 31

Figure 17. Control configuration for system frequency response characterization. Low-level PID control (orange) was run on the drive for position input tracking. Desired positions P_d are input to the motor drive, and tracked in a cascaded PID loop, depicted as the simplified feedback loop with encoder gain K_e and measured motor encoder position P_e . The actual motor position P_m is transmitted through the knee brace to the user, and the resulting knee brace BAM τ_{kb} measured with load cell K_{kb} 36

Figure 18. Bode plot for discrete sinusoidal 1-12 Hz motor position inputs to knee brace BAM output. 40

Figure 19. Select experimental conditions for comparison of Peak BAM magnitude and walking speed effect on trajectory tracking results. Condition 3 is 115 %WS 8.1 Nm peak BAM, 4 is 85 %WS with 2.7 Nm peak BAM, and 9 is 100 %WS with 5.4 Nm peak BAM. Lines are averages across steps and shaded regions are \pm one standard deviation..... 41

Figure 20. Experimental conditions for comparison of gait kinematic effects. Walking TT is trajectory tracking at 100 %WS 4.1 Nm peak BAM, Stationary TT is 4.1 Nm peak BAM while stationary, and Walking CP is 100 %WS with constant motor position. Lines are averages across steps and shaded regions are \pm one standard deviation..... 43

LIST OF TABLES

Table 1. System performance specifications.	14
Table 2. Major ABLE system components.....	15
Table 3. Motor trajectory simulation results used for motor selection.....	20
Table 4. Analysis approach for motor transmission.	22
Table 5. Key evaluation questions.....	34
Table 6. Human subject test conditions. Crossed cells indicate no value.....	35
Table 7. System performance specifications with results from associated test conditions.	39
Table 8. Trajectory tracking RMS error results for conditions of varying walking speed and peak BAM magnitude. Crossed cells indicate untested condition.	41

LIST OF ABBREVIATIONS

KOA	Knee osteoarthritis
TKA	Total knee arthroplasty
KAM	Knee adduction moment
MCF	Medial contact force
BAM	Brace abduction moment
ABLE	Active brace for laboratory exploration
OTS	Off-the-shelf
FFT	Fast Fourier transform
DC	Direct current
PSU	Power supply unit
BOM	Bill of material
%GC	Percent gait cycle
GRF	Ground reaction force
CPU	Central processing unit
BMI	Body mass index
IRB	Institutional review board
RMS	Root mean square
%WS	Percent walking speed

ACKNOWLEDGEMENTS

This work was completed with support from the Veterans Affairs Center for Limb Loss and Mobility staff, resources, and funding, and Amplifying Movement and Performance Lab funding.

Chapter 1. INTRODUCTION

1.1 *Knee Osteoarthritis Background*

Knee osteoarthritis (KOA), a chronic degenerative disease, affects at least 7% of US adults older than 45 years, and at least 12% of US adults older than 60 years [1]. KOA is the most common joint disease, and one of five leading causes of pain and disability in non-institutionalized adults [2], [3]. Although numerous conservative treatment strategies exist, total knee arthroplasty (TKA) is often required in the end stages of KOA [4].

The economic burden of KOA is significant. Surgical procedures contribute the greatest cost to KOA treatment [5]. In 2011 Medicare reimbursed \$3.5 billion for TKA, the largest expenditure for a single procedure. The estimated cost for primary TKA is \$20,700 and revision TKA is \$24,500 per procedure [6]. These costs coupled with population aging, rising KOA prevalence, and the volume of surgical procedures yield a significant economic burden. Improved early conservative KOA interventions could mitigate this trend.

1.2 *Knee Loading*

Contact forces within the knee joint are thought to contribute to KOA disease development and progression. The medial compartment of the knee typically has the highest loading and is also the most commonly affected by KOA [7]. Due to the difficulty in measuring medial contact forces, the knee adduction moment (KAM) is often used as a surrogate measure. The reliability of KAM as a medial contact force (MCF) surrogate is not well understood, where studies have found KAM to be an insufficient regressor for MCF alone [8]–[11]. Additional potential predictors of MCF include gait type [9], foot angle [12], and mechanical knee joint axis [10]. Unloader braces, a common conservative treatment strategy, target KAM reduction by applying an abduction moment

through a wearable device. This thesis focuses on creating a tool for investigating improved wearable device treatment strategies.

1.3 Medial Unloader Braces

Medial unloader knee braces (Figure 1) are commonly prescribed to reduce joint loading and manage pain [13]. These braces generate a brace abduction moment (BAM) to counteract the knee adduction moment (KAM) to decrease medial compartment loading. However, evidence of brace efficacy is inconclusive and limited by user compliance. Dr. Duivenvoorden concluded that evidence of unloader brace benefit was inconclusive for quality of life, pain, and function improvement in the 2015 Cochrane Systematic Review [14]. Dr. Squyer found that patients have a low likelihood of using their brace more than one year after prescription in a survey-based study of n=89 brace users [15].

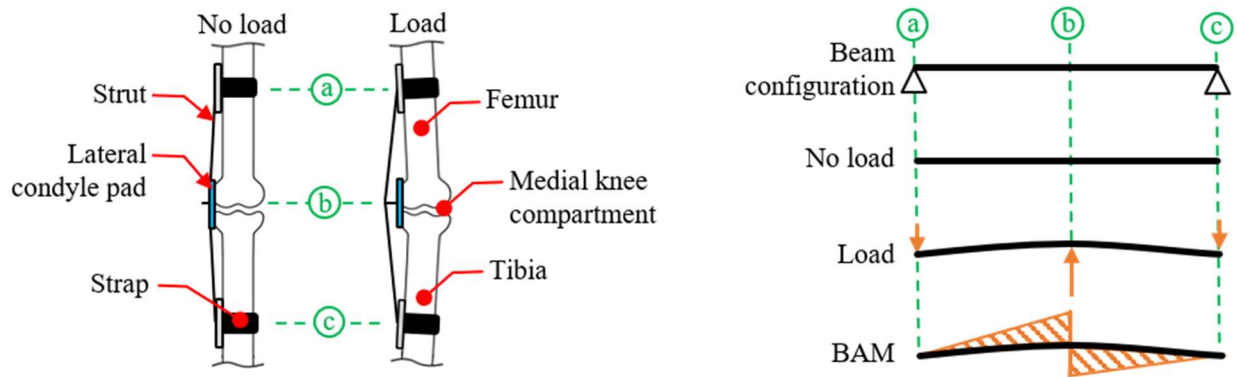


Figure 1. Common medial unloader brace design with three-point bending principle. Strut bending (shown in the ‘Load’ state) generates an abduction moment. The strut is bent when the applied force at the lateral condyle pad is reacted by strap grounding interfaces on the femur and tibia. Load is applied when the condyle pad is translated toward the knee in the medial direction. The loading states and generated BAM are depicted with the classical mechanical embodiment of simply supported beam with central load. Maximum BAM is reached at location ‘b’, the lateral condyle pad.

Existing unloader braces are simple, passive devices with numerous shortcomings. For example, these braces apply the same BAM regardless of the user's activity (e.g. sitting, standing, fast or slow walking). Passive braces cannot adapt to situations where the BAM is too low or too high for a given activity. Brace slippage and strap loosening can result in decreased BAM that doesn't protect the knee. These factors may affect brace efficacy and lead to poor user compliance.

1.4 *Powered Assistive Devices*

Pneumatic unloader braces have been investigated with the aim of improving patient brace adoption [16], [17]. These devices targeted typical brace structure and loading scheme improvement by using soft structures in place of typical rigid frame designs, and air bladders in place of less compliant translating condyle pads. An example device is shown in Figure 2. In both studies, a constant pressure was used throughout the gait cycle, akin to common commercial braces designed to maintain a constant setting, typically lateral condyle pad position or brace valgus angle.



Figure 2. Pneumatic unloader brace with soft structure studied in [17]. Arrows point to air bladder locations used to generate BAM when inflated. Figure is copied from [17].

Numerous powered assistive devices have been developed and investigated for controlling torques at the knee and ankle in the sagittal plane. With the speeds, torques, sensing, and computation required to carry out biomechanical trajectories, offboard systems have been developed to separate wearable devices from typically bulky actuation and control components [18]–[20]. Offboard systems aim to decouple the wearable device design from experimental investigation, where a lightweight wearable prosthesis or orthosis and oversized offboard system are developed to emulate a wide range of passive and active device embodiments, enabling subsequent investigation in a larger (than that of an onboard actuated system) solution space.

1.5 PURPOSE

The purpose of this study was to develop a robotic knee brace capable of modulating frontal plane BAMs during the gait cycle in a laboratory environment. The system is intended as a tool for exploring active unloader brace operation to inform the investigation of novel KOA treatment

strategies. To this end, a lightweight wearable knee brace and off-board actuation system were developed, and its performance evaluated for various unloading conditions. Testing was performed to compare results to engineering specifications established during design, and answer key questions about the inputs that affect trajectory tracking performance during steady state walking. Taken together, the evaluation is intended to give a qualitative and quantitative understanding of both system behavior and system capability as a research tool. A system overview is presented in Chapter 2, the design and evaluation of the mechatronic and control systems in Chapters 3-4, followed by preliminary human subject testing in Chapter 5.

Chapter 2. SYSTEM DEVELOPMENT

2.1 *System Definition*

We propose that improved KOA intervention exists in a large multidimensional space of brace design and BAM modulation pattern. ABLE (active brace for laboratory exploration) was developed to explore that space. It is intended to modulate medial knee compartment load during gait with flexible, user defined inputs. To this end, engineering specifications (Table 1) were derived from assumed biomechanical requirements for modulating medial knee compartment load. Their derivation is summarized below.

Table 1. System performance specifications.

Description	Specification
Peak BAM	≥ 7 Nm
Bandwidth	≥ 10 Hz
Range of motion	$\geq 120^\circ$

Peak BAMs of 0.04 to 0.065 Nm/kg have been reported for passive commercial braces in previous studies [21], [22]. Assuming 100 kg user yields peak BAM requirements of up to 6.5 Nm. To our knowledge, no model for, nor rule of thumb, exists for a quantitative selection of BAM magnitude. In real-world daily use, braces are set by patients based on internal subjective measures such as relief, pain, and comfort. A peak BAM of 7 Nm was selected as a conservative specification to encompass the potential range of patient selected unloading levels.

The bandwidth requirement is defined for BAM modulation (trajectory tracking control) functionality. During steady state walking, 99.7% power of toe and heel trajectory signals is contained below 6 Hz, where toe and heel trajectories exhibit the highest harmonics [23]. Bandwidth was conservatively set to 10 Hz to control the additional dynamics we introduce when modulating BAM at higher rates than gait trajectories.

The system was realized as a knee brace coupled via a Bowden cable to an off-board actuation system, where a Bowden cable is a tendon-sheath system with rope (tendon) routed through flexible housing (sheath) that transmits load from the motor to the knee brace. This separation of wearable and actuation components is intended to maximize wearable device biomechanical transparency and lower development barriers to the scientific evaluation of active bracing in KOA. The over-design of actuation components, where a large servo motor and real-time controller provide excess mechanical and computational power, simplifies knee brace, actuation, and control development. The selected major system components are summarized in Table 2; their development is detailed in subsequent sections of this chapter.

Table 2. Major ABLE system components.

Sub system	Description	Make/model
Knee brace	Knee brace	Ottobock/Agilum Reactive
	Unloader mechanism	Custom
	Load cell	Omega/LC202
Off-board system	Real-time controller	National Instruments/cRIO
	Motor drive	Kollmorgen/AKD-P00606
	Servo motor	Kollmorgen/AKM-52H
	Motor chassis	Custom
	Host computer	Windows PC

2.2 Knee Brace Design

An off-the-shelf (OTS) knee brace (Ottobock *Agilum Reactive*) was modified with a custom mechanism to allow for BAM modulation via a Bowden cable. The OTS brace (Figure 3) operates using the components and 3-point bending configuration summarized in Figure 1. In typical commercial braces, load modifying settings are fixed during gait; the robotic knee brace allows for continuous, dynamic translation of the condyle pad via a custom mechanism.



Figure 3. Unmodified OTS brace, Ottobock *Agilum Reactive*. BAM is generated via rotation of a screw which increases the valgus angle between the thigh and shank sections. This functionality is modified in the developed knee brace.

A custom mechanism that translates Bowden cable force into condyle pad motion was designed and fit to a modified OTS brace (Figure 4). The Ottobock *Agilum Reactive* brace was selected for sizing and material: it is designed as a one-size-fits-all device, and the majority of the structure is machinable. BAM modulation functionality is achieved through two primary components in the mechanism: a shaft grounded to the polycentric knee joint of the brace, and a housing which slides along the shaft to which the condyle pad is affixed. The Bowden sheath terminates at the housing, and tendon at the shaft, to yield the desired relative motion between the two components.

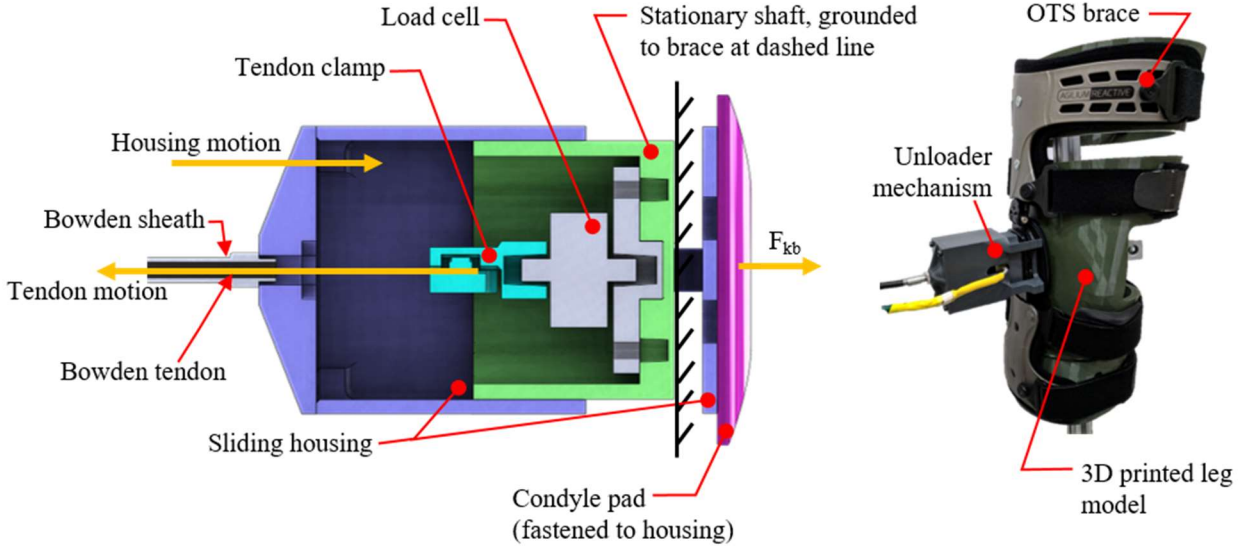


Figure 4. Knee brace design, shown as the developed knee brace (right) and section view of the unloader mechanism 3D model (left). Tendon motion relative to the sheath generates an equal and opposite knee brace force F_{kb} at the condyle pad which contacts the medial side of the knee. The 3D printed leg model was used for control law and safety system development to prepare for human subjects testing.

A load cell is incorporated between the tendon and shaft to directly measure force transmitted to the participant and compute the resulting BAM (Equation 1).

$$BAM = F_{kb} \left(L_{ls} - \frac{L_{ls}^2}{L_{kb}} \right) \quad (1)$$

BAM is computed with the force measured at the load cell F_{kb} , the total knee brace length L_{kb} , and the length from the lower strap to the condyle pad center L_{ls} . The relationship is derived from a simply supported beam with a single point load F_{kb} .

2.3 Off-board System Overview

A servo motor generates Bowden cable force through a custom chassis. The motor is controlled by a real-time controller (National Instruments cRIO) and drive (Kollmorgen AKD). The controller performs sensor input/output, high-level control, and custom real-time tasks, while the

drive manages low-level motor control. A host computer connected to the controller performs non-time critical tasks such as data logging, user interface, and system management. The system is housed in a custom cart constructed from t-slotted framing components (Figure 5).

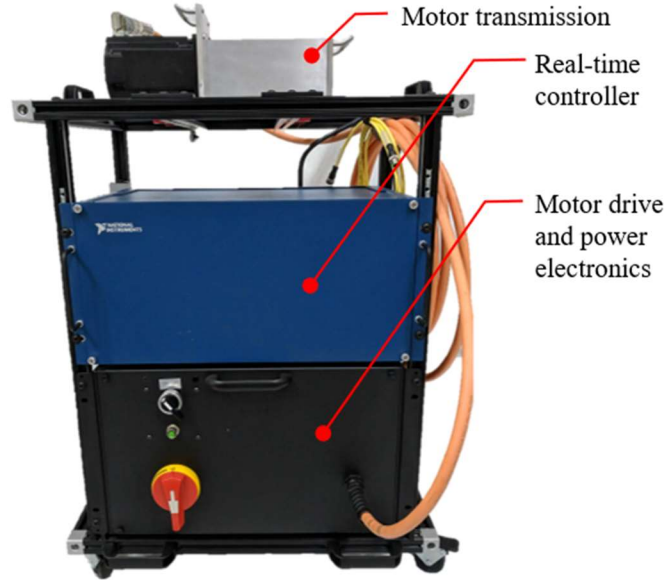


Figure 5. Off-board system construction, host PC not shown. Although the host PC is required per the developed program architecture, its performance does not impact real-time control tasks.

Motor selection, chassis design, and drive power circuit design are detailed in the following sections of this chapter.

2.4 *Motor selection*

A motor was selected based on simulation of a simplified dynamical model of the knee brace and motor. Simulation was performed with the dynamical model of Equation 2.

$$\tau_m = S_f(\bar{I}\alpha + \tau) \quad (2)$$

where τ_m is motor torque required, \bar{I} is the rotational inertia of the system, S_f is a safety factor, α is angular acceleration, and τ is torque. Torque (Equation 3) was represented as a function that maps the desired BAM versus gait cycle trajectory at the knee brace, τ_d , to motor torque, τ , via

brace geometry (L_{ls}, L_{kb}) and motor sheave diameter D_s - a motor transmission component about which Bowden cable tendon is wrapped.

$$\tau = f(\tau_d, L_{ls}, L_{kb}, D_s) \quad (3)$$

The angular acceleration required to carry out the desired torque trajectory (Equation 4) was represented as a function of desired BAM trajectory, brace geometry, system compliance K_{eff} and motor sheave diameter.

$$\alpha = f(\tau_d, L_{ls}, L_{kb}, K_{eff}, D_s) \quad (4)$$

Brace geometry maps the desired BAM trajectory to cable force, system compliance maps cable force to motion, and the sheave maps linear cable to rotary motor motion, yielding motor angular acceleration. System compliance was modeled as a series spring comprised of the brace and cable. Given the simplifying assumptions, a safety factor of five was used to account for unmodeled dynamics such as Bowden cable friction, soft tissue compliance, and leg volume changes.

Numerical simulations of Equations 2, 3, and 4 were carried out in MATLAB to determine the motor torque and velocity required to achieve the desired BAM trajectory for catalog motor inertias. Worst case conditions of performance specifications in Table 1 were used with assumed brace compliance and 1 Hz gait cycle. Desired torque and acceleration were computed based on a 1-8 Nm BAM profile range, 1 Hz step frequency with swing and stance phases of 40% and 60% of gait cycle, respectively. Sheave diameter was conservatively set to 1.5 in. Rotational inertias from Kollmorgen motor catalogs were used and scaled by a factor of 1.2 to account for the additional transmission components required to convert motor rotational to linear cable motion. The resulting motor trajectory that achieves the input BAM trajectory at the knee brace is shown in Figure 6.

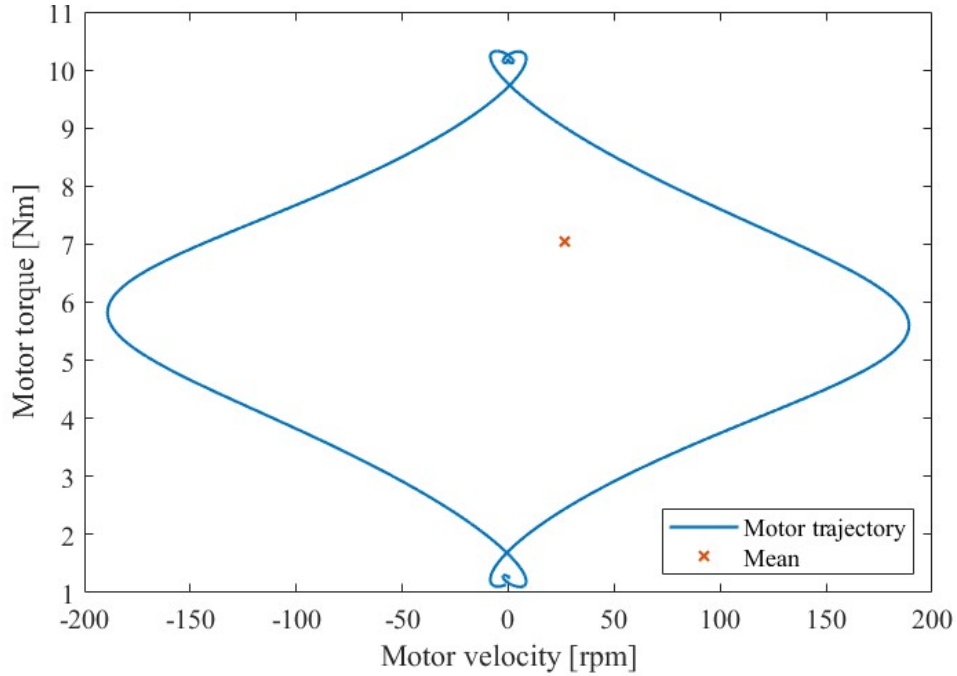


Figure 6. Motor torque-speed trajectory for the input BAM versus percent gait cycle trajectory.

The following criteria were evaluated to select the motor:

- $\text{mean}(\tau_m) < \text{catalog continuous rated torque}$
- $\text{max}(|\omega_m|) < \text{catalog rated speed}$
- $\text{max}(\tau_m) < \text{catalog peak rated torque}$

The simulated motor trajectory used for the evaluation are listed in Table 3.

Table 3. Motor trajectory simulation results used for motor selection.

Description	Result
Continuous torque	7.0 Nm
Peak torque	10.3 Nm
Speed	189 rpm

Forty-six motors were compared to the above inequality constraints. The Kollmorgen AKM-52H, the motor with the lowest inertia that met the constraints, was selected for use in the off-board actuation system. The MATLAB code used to perform the numerical simulation including the input BAM trajectory used, are attached as Appendix A.

2.5 Motor transmission design

A custom transmission was designed to ground the motor and translate rotary motor into linear cable motion (Figure 7).

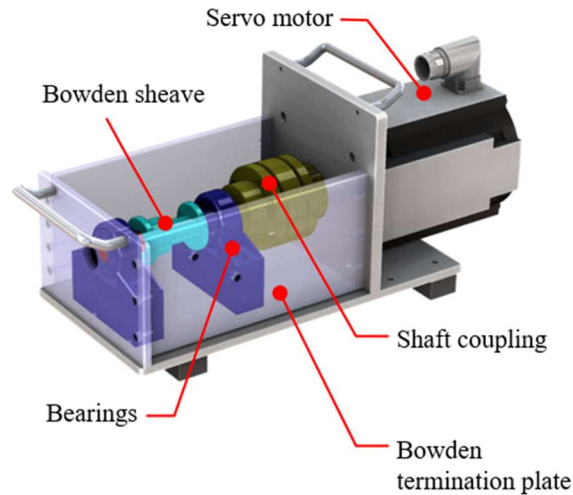


Figure 7. Motor transmission. Bowden cable sheath (not shown) terminates at the ‘Bowden termination plate’, and cable tendon is wrapped around the sheave.

Cable tendon is coupled to the motor through a 3D-printed sheave on a shaft supported by pillow-block bearings at opposite ends. The shaft is driven by the motor through a flexible coupling. This configuration reduces radial load on the motor bearings generated by the cable and connected orthosis. The flexible coupling allows for inherent misalignment of the shaft and motor rotational axes due to uncertainty in machining and assembly while maintaining desired torsional stiffness. These motion components are oriented by a machined aluminum frame.

Attributes expected to affect system dynamics were designed to be easily adjusted, or tuned, for subsequent design-test iterations inherent to the development process. Considering sheave design, the ratio of sheave diameter to brace condyle pad travel is the effective gear ratio of the system, and the method for adequately tensioning and aligning the cable was not known during the initial design phase. A 3D printed sheave was used to expedite design-test iterations,

and a D-profile shaft for 3D-printed sheave implementation, where the ‘D’ cross section constrains rotation through geometry.

An outline of the motor transmission specification methodology is listed in Table 4.

Table 4. Analysis approach for motor transmission.

Description	Analysis
Shaft coupling	Comparison of manufacturer motor and coupling specifications
Bearings	
Shaft	Stress analysis from first principles
Plates of transmission frame	Material selection: thermal analysis from first principles
	Sizing: conservatively oversized using engineering acumen
Fasteners to mate frame plates	Stress analysis from first principles

All stress analysis was performed with outputs as discrete variables, taking on values of OTS stock sizes, e.g. analysis was performed for shaft sizes of ¼ and ½ in. Shaft sizing is outlined below and detailed in Appendix B. Frame analysis is restricted to Appendix B only.

Stresses were computed for the shaft in torsion and bending. Torsion τ_t was computed using Equations 5-6 from [24].

$$\tau_t = \frac{TB}{r^3} \quad (5)$$

where T is the applied torque, r is the shaft radius, and B varies with $h = 1 - \cos\alpha$.

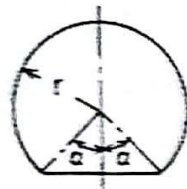


Figure 8. D-profile shaft cross section parameterization. Image copied from [24]

$$B = 0.64 + 1.76h - 5.49h^2 + 14.06h^3 - 14.51h^4 + 6.43h^5 \quad (6)$$

The peak motor torque of the selected Kollmorgen motor was used for the applied torque. Shaft bending stress was computed assuming a circular cross section, which is worst case compared to

a D cross section. Normal (bending) and shear (torsional) stresses were combined with plane stress Equation 7.

$$\sigma_p = 0.5 \left(\sigma_{bend} + \sqrt{\sigma_{bend}^2 + 4\tau_t^2} \right) \quad (7)$$

where σ_{bend} is the bending stress, and σ_p is the combined principal stress. Safety margins S_m were computed for a range of diameters with Equation 8.

$$S_m = \frac{\sigma_y}{\sigma_p} \quad (8)$$

where σ_y is the yield stress of the shaft material, selected to be stainless steel. Results are shown in Figure 9.

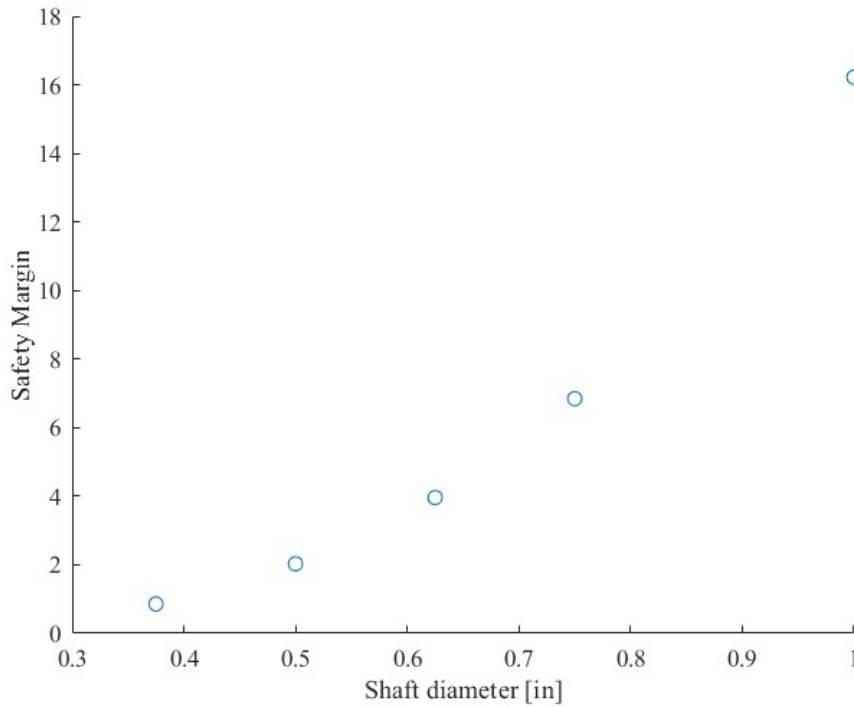


Figure 9. Safety margins for shaft sizing analysis based on combined principle stress from bending and torsion.

A shaft diameter of 0.625 in with a safety margin of 4.0 was conservatively selected. All analysis was performed in MATLAB R2018b with code attached in Appendix B.

2.6 Drive power circuit design

A circuit was designed and implemented in an enclosure to power the motor drive (an OTS component). The developed sub-system is shown in Figure 10.

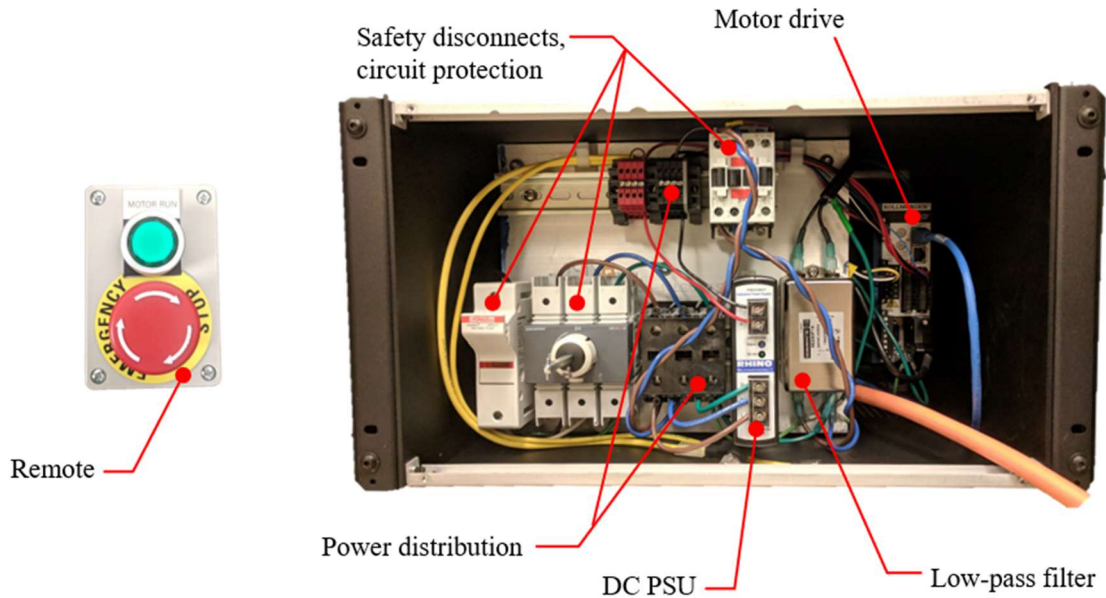


Figure 10. Motor drive power circuit (right) in rack-mountable enclosure and remote (left). The direct current power supply unit (DC PSU) powers the logic circuit which controls high level motor commands such as emergency stop, system on/off, etc. Both the remote and drive circuit are custom components.

All components, e.g. filter, DC PSU, were selected and installed per drive manufacturer specifications and intended use. The remote was added for safety and ease of use. The diagram of the designed circuit and associated bill of material (BOM) are included as Appendix C.

Chapter 3. SOFTWARE AND CONTROL LAW DEVELOPMENT

Software was developed to achieve the desired BAM modulation functionality and manage experimental tasks such as data logging and visualization. Software was developed for the distributed architecture (Figure 11) of host PC, real-time controller, and motor drive, where each executes specialized tasks for which each system is designed.

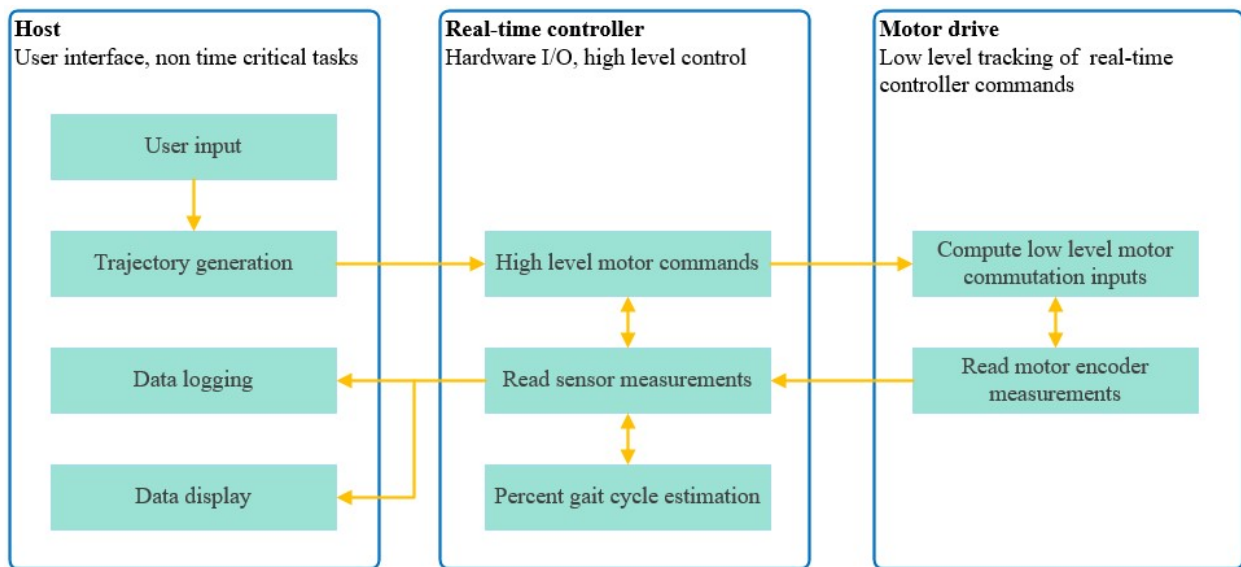


Figure 11. ABLE software architecture. The host PC is used to interact with the system and perform non time critical tasks like data logging, the real-time controller performs time critical computation such as sensor input/output and motor control inputs (velocities), and the motor drive runs its own control law for tracking the desired motor velocities. The architecture was implemented in LabVIEW 2018.

A control law (Figure 12) was designed within the architecture to track a BAM profile over percent gait cycle (%GC). Its design is described in the subsequent sections of this chapter, in order of real-time execution: §3.1 Trajectory Generation, §3.2. Percent Gait Cycle Estimation, §3.3. Compensation. Trajectory generation is performed at system start, while the subsequent steps are executed every control loop iteration at 200 Hz. Initial development was performed on a benchtop system prior to human subject testing.

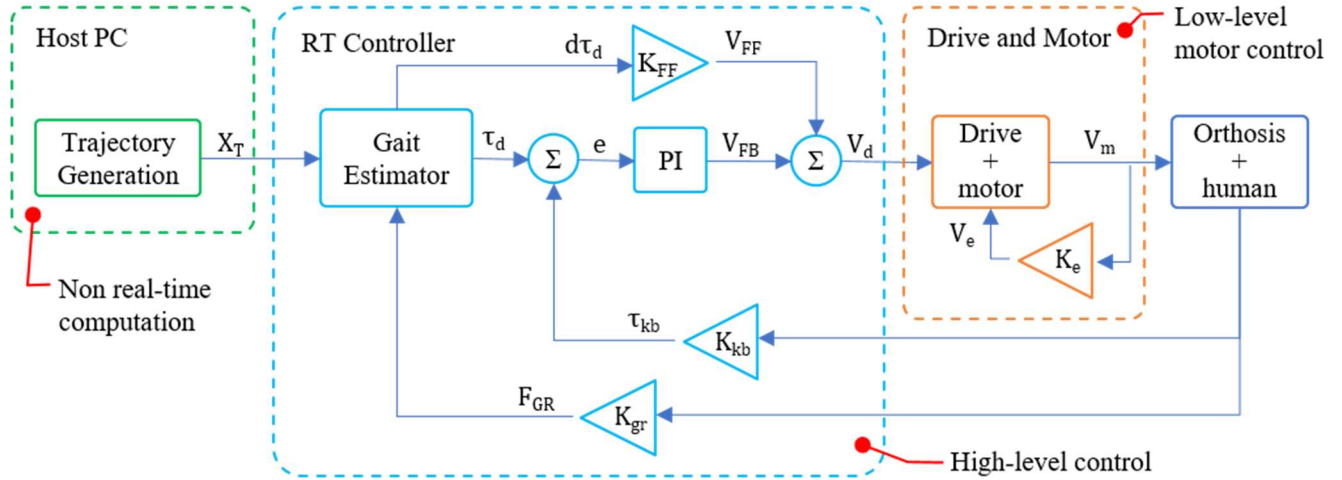


Figure 12. Simplified control law design and distributed system implementation. Following initial trajectory X_T generation, the current %GC is estimated and reference BAM values passed to each compensator path: the desired BAM change $d\tau_d$ and desired BAM τ_d to the feedforward and feedback compensators, respectively. The feedforward control input V_{FF} is computed as the product of desired BAM change and feedforward gain K_{FF} . The feedback control input V_{FB} is computed from the error e between desired BAM and knee brace BAM τ_{kb} using a proportional-integral compensator PI. The motor drive, running a cascaded proportional-integral-derivative loop (shown in a simplified feedback form), tracks input desired velocity V_d from encoder measurement V_e and outputs motor velocity V_m . Sensor calibration constants are modeled as gains K_e , K_{kb} , and K_{gr} , for the motor encoder, knee brace load cell, and treadmill ground reaction force plate, respectively.

3.1 Trajectory Generation

The BAM vs %GC trajectory (Figure 13) is parameterized as four sections: rise from minimum to peak BAM, hold at peak BAM, fall to minimum BAM, and hold at minimum BAM. The rise is intended to coincide with KAM increase following heel strike and fall with the start of swing phase. It is the final section, hold at minimum BAM, that differentiates the unloading behavior of ABLE from a typical passive brace, where a passive brace maintains a consistent BAM throughout stance and swing. This trajectory serves as a starting point for system development; trajectory

generation is designed as a modular software component to ease investigation of novel unloading schemes.

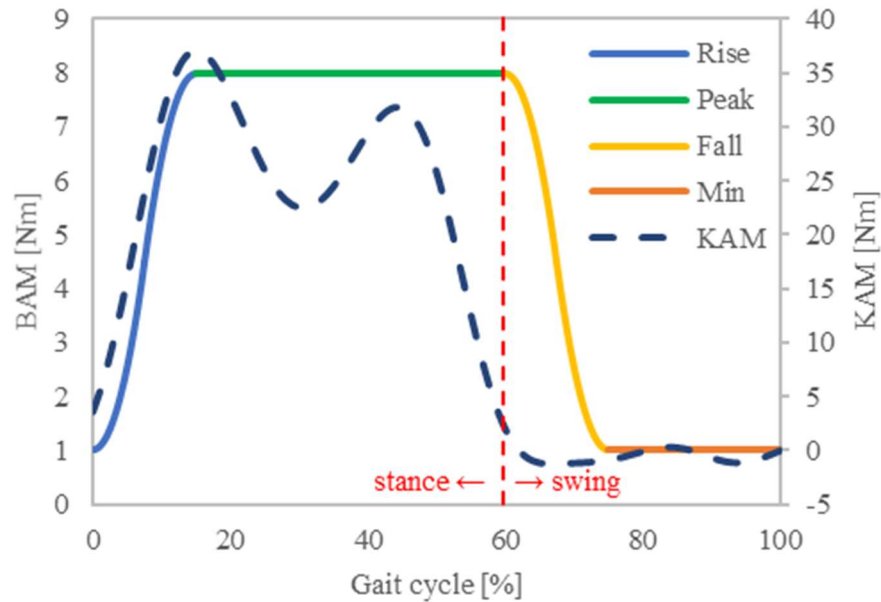


Figure 13. Example computed BAM trajectory with 0-15% gait cycle rise to 8 Nm peak BAM and 60 to 75% fall to 1 Nm minimum BAM. The average KAM is shown for a 100 kg healthy adult during level ground treadmill walking [15]. BAM is intended to reduce the KAM acting on the internal medial compartment, where BAM and KAM act in opposite directions: BAM in abduction, and KAM in adduction.

A smooth trajectory is desired for user comfort and motor life. To find smooth transitions from minimum to maximum BAM, the rising and falling sections are each defined by a concave up and concave down C^2 function of equal curvature, with the functions connected at their joint inflection point. The entire trajectory is found online analytically per user input parameters of minimum BAM, peak BAM, and percent gait cycle transition points, then discretized at the desired sampling rate. The trajectory generation routine was developed in MATLAB and is attached with an example trajectory in Appendix D.

A trajectory defined minimum BAM value is essential for stable performance given the physical system embodiment. The Bowden cable can only load the knee brace in tension, meaning

it can only drive system load in the positive direction; dynamics in the negative direction are governed by passive brace compliance. It follows that when relaxed, the system is dominated by nonlinear behavior, which would lead to undesirable control performance, i.e. when the system is not in tension, the system output (BAM) is poorly correlated with the input (motor motion).

3.2 Percent Gait Cycle Estimation

The reference BAM trajectory is defined on a periodic basis of %GC. An algorithm was designed to estimate %GC in real-time from vertical ground reaction force (GRF) measurements of the ipsilateral limb. A high-level description of algorithm function is described below, and an iterative description shown in Figure 14.

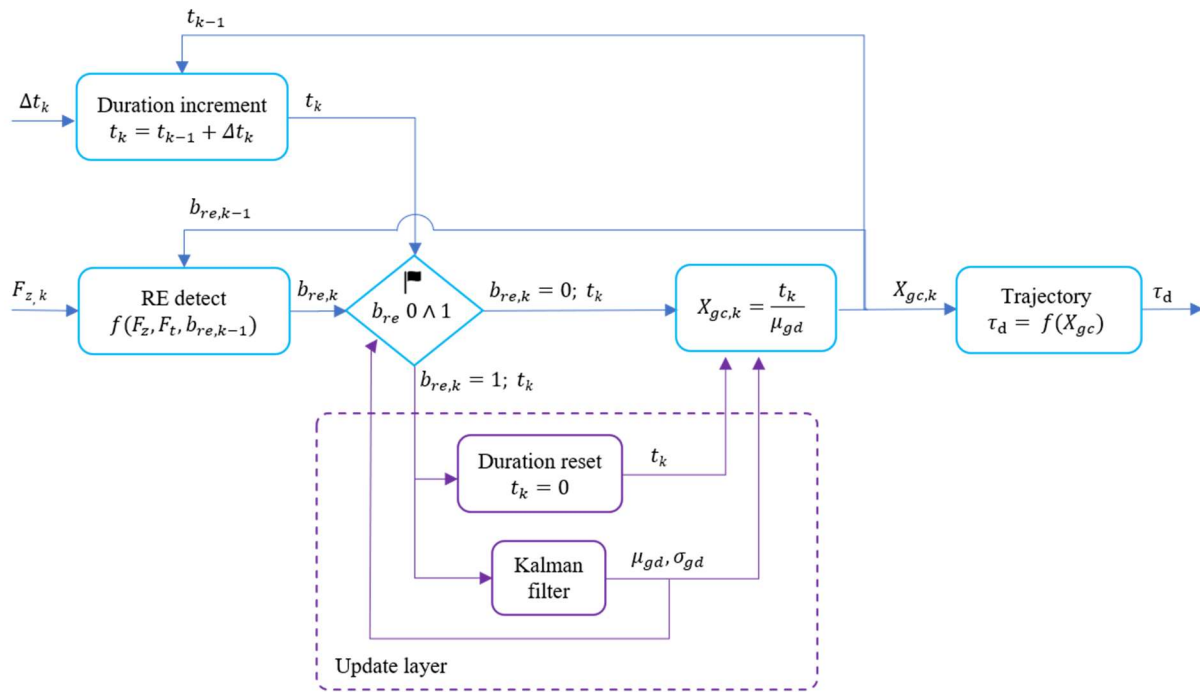


Figure 14. Gait cycle estimation algorithm design. The iterate index k refers to the current loop iteration and $k - 1$ to the previous. At each loop iteration, the time elapsed since the previous loop cycle, Δt_k , is input from the CPU clock, and vertical GRF, $F_{z,k}$, from the instrumented treadmill force plate of the braced leg. Vertical GRF is thresholded and compared to the previous state to find rising edges in the signal and thus whether heel strike has

occurred - the output is a binary bit $b_{re,k}$. The diamond shaped block performs a flagging operation and acts as a gate, switching between two paths $b_{re,k} = 0$ for no rising edge/heel strike event and $b_{re,k} = 1$ for the occurrence of a rising edge event. The flagging operation filters for false heel strike events by evaluating Equation 7. If no rising edge is detected ($b_{re,k} = 0$, most loop iterations), then the routine bypasses the update layer, computes percent gait cycle $X_{gc,k}$, and finds the desired BAM τ_d from the trajectory, a transfer function from $X_{gc,k}$ to τ_d . When rising edges are detected, the current time duration t_k is passed to the Kalman Filter to update the gait cycle mean μ_{gc} and standard deviation σ_{gc} estimates, and t_k is reset to zero before computing $X_{gc,k}$.

The algorithm takes in real-time computer clock cycle counts and vertical GRF measurements, estimates a gait cycle duration, and outputs a desired BAM. The start of the gait cycle is defined by heel strike, obtained from a threshold on vertical GRF. At heel strike a high-resolution counter increments in time and is reset at the following heel strike, giving a time duration measure of each gait cycle. The gait cycle duration is parameterized by a Gaussian and estimated using a plain Kalman Filter. The %GC is computed as

$$X_{gc} = \frac{t}{\mu_{gd}} \quad (9)$$

where X_{gc} is the percent of the current gait cycle, t is the time elapsed from the previous heel strike, and μ_{gd} is the estimated mean gait duration updated using the Kalman filter.

As the system is initially intended for steady state walking on an instrumented treadmill, vertical GRF data was obtained from readily available force plate measurements. To mitigate false heel strike detections, the following constraint is evaluated at each event.

$$\mu_{gd} - 3\sigma_{gd} \leq t \leq \mu_{gd} + 3\sigma_{gd} \quad (10)$$

where σ_{gd} is the estimated gait duration standard deviation updated using the Kalman filter. The event is discarded if the condition is not met.

For this KOA unloading application, accurate estimation is most critical as the ipsilateral knee is loaded following heel strike, i.e. for the building of brace load to align with that of the knee. The algorithm design is biased to robustly detect heel strike events, and thus align the increase in BAM with increase in KAM of the braced limb.

3.3 *Compensation*

The control law is a two degree of freedom system with feedforward and feedback compensation paths [25]. This design separates the trajectory tracking problem into trajectory (feedforward) and error (feedback) tracking. A scalar gain is used in the feedforward path and proportional-integral controller in the feedback path. The scalar feedforward gain was implemented due to the piecewise linear relationship between motor position change and BAM change found during benchtop testing. Control inputs are computed as motor velocity commands, the input to the feedforward gain is a change in BAM, and the output a change in motor position.

The relationship between constant motor inputs of torque and position, and output of BAM were evaluated during bench top testing. With the brace donned on the 3D printed leg model (shown in Figure 4) the motor drive was set to a position or torque loop mode and the input ramped positively to a peak value, then negatively to the initial value. The BAM output was computed at each input value from load cell measurements. The resulting torque input to BAM output is shown in Figure 15, and position to input to BAM output in Figure 16.

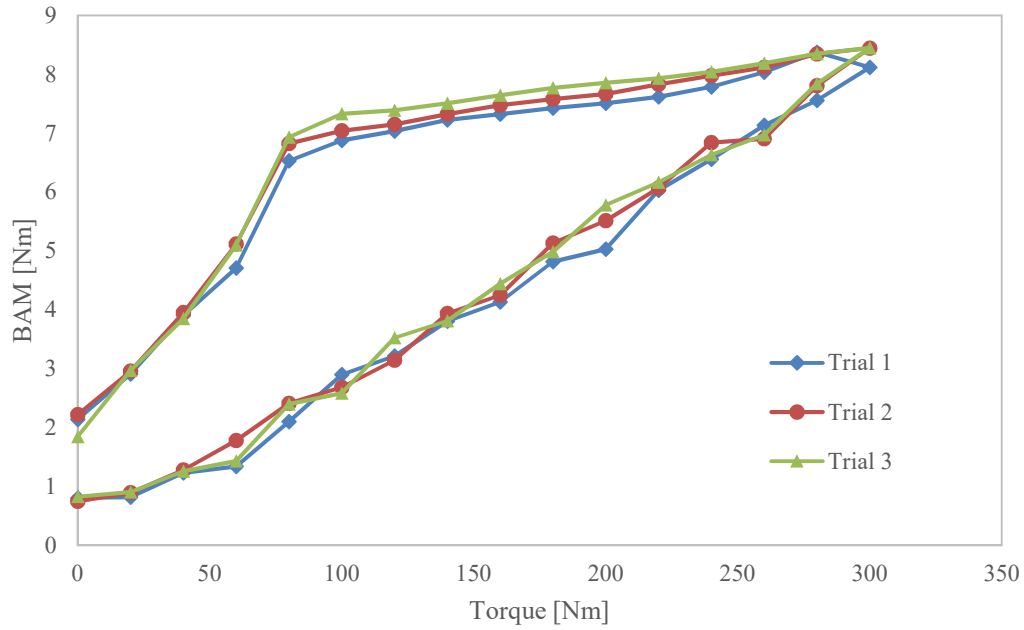


Figure 15. Motor torque inputs to BAM output for n=3 trials. The initial point for all trials is the minimum BAM value at 0 Nm motor torque, i.e. the lower of segment of each trial corresponds to increases in motor torque.

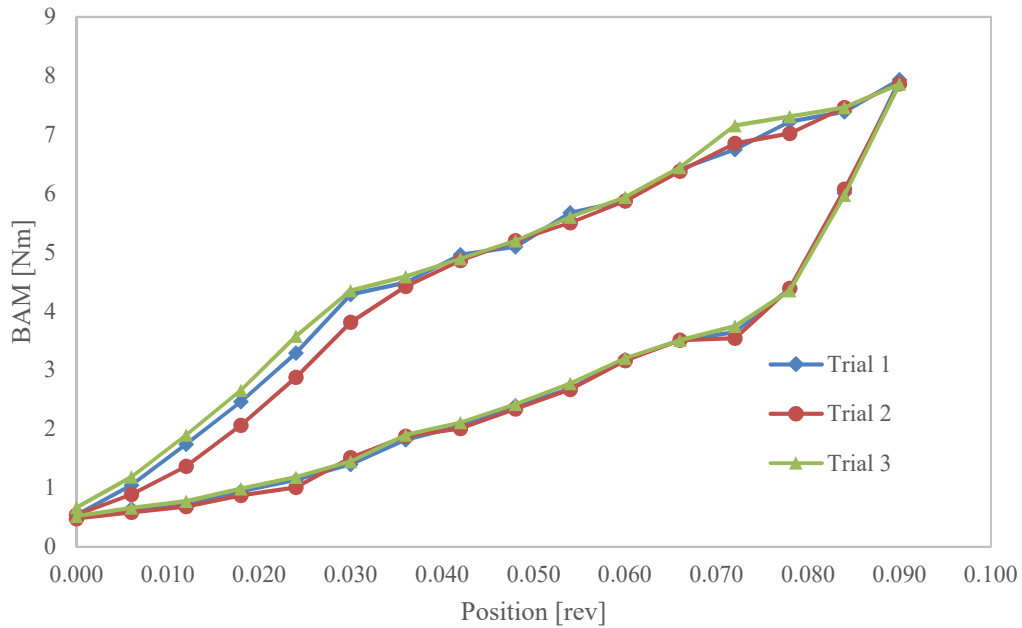


Figure 16. Motor position inputs to BAM output for n=3 trials. The lower segment of each trial corresponds to increases in motor position, while the upper segment corresponds to decreases.

Both position and torque inputs exhibited hysteresis during brace loading, which is expected to result from Bowden cable mechanics. The relationships, however, differed in shape where the hysteresis of the torque input resembles a triangle, and position a parallelogram. The difference in shape is expected to be a result of control architecture and brace mechanics. The motor torque control loop is subject to deadband, where a minimum torque threshold is required to overcome motor stiction, motor inertia, and Bowden cable friction. Based on the three-point bending design of the brace, BAM is expected to be correlated with compliance, where linear translation of the condyle pad yields a proportional change in BAM. It is the transfer function relationship between motor output and BAM by which the behavior of the two control loops differ. Assuming 1:1 motor input to output (a perfect motor control loop tuning), in torque mode Bowden cable motion, or position change, at the motor is dependent on the three high-level parameters: the torque input, load at the knee brace, and load in the Bowden cable; whereas in position mode cable motion at the motor is dependent on one parameter: motor position input. In other words, by tracking positions in a system where the output of interest, BAM, is strongly dependent on position change, the position motor control loop compensates for some undesirable motor and Bowden cable behavior that affects the relationship between motor output, cable translation, and resulting BAM change.

The behavior of the position input-output relationship is more desirable from a control perspective. Considering the position to BAM curve as a parallelogram, it is comprised of two slopes, meaning that motor position change to BAM change is equivalent for sections of equivalent slope, i.e. monotonic changes in BAM correspond to equivalent changes in motor position regardless of whether BAM is increasing or decreasing. The motor control mode was thus selected to be velocity (position change), and the average of the slopes of the motor position to BAM curve

used in the feedforward gain path. Tracking performance could later be improved by including a position to BAM model and system compliance model in the feedforward path.

Chapter 4. METHODS: HUMAN SUBJECT TESTING

Human subject testing was performed to evaluate the system from two perspectives: a formal comparison of results to performance specifications, and to answer key questions about system behavior. Performance specifications were previously stated in Table 1 in §2.1 System Definition, and pertained to system peak BAM output, bandwidth, and brace range of motion. Key questions are listed below in Table 5.

Table 5. Key evaluation questions.

Number	Question
1	How does the RMS BAM tracking error vary with walking speed and trajectory peak BAM magnitude?
2	What is the effect of walking on trajectory tracking BAM output compared to stationary trajectory tracking BAM output?
3	How are the brace users' natural gait kinematics affecting BAM output?

The intention of question one is to characterize trajectory tracking error over a range of assumed significant inputs (walking speed and peak BAM). Although performance specifications were not set for tracking error, it is considered valuable for understanding the behavior of the developed system. Questions two and three focus on gait kinematics; they are posed to observe the system dynamics to which controller is responding. Answers to these questions paired with comparison of results to performance specifications is intended to give a qualitative and quantitative understanding of both system behavior, and system capability as a tool for investigating conservative medial KOA treatment.

One healthy male subject, BMI 22, was recruited for this IRB approved study at the VA Puget Sound Health Care System. Following knee brace fitment by a certified orthotist, eleven conditions varying in input type, walking speed, and peak BAM were tested to compare actual system performance to target design specifications (Table 1), and answer key evaluation questions

(Table 5). Conditions are listed in Table 6 with the associated performance specifications and key questions for which each condition was tested.

Table 6. Human subject test conditions. Crossed cells indicate no value.

Condition	Reference Signal	Walking speed [% nom]	Peak BAM [Nm]	Performance spec	Key question
1	Motor position Sinusoid	Stationary	N/A ^a	Bandwidth	
2	Trajectory	100%	8.1	Peak BAM	1
3	Trajectory	115%	8.1		1
4	Trajectory	85%	2.7		1
5	Trajectory	Stationary	4.1		2
6	Trajectory	85%	4.1		1
7	Trajectory	100%	4.1		1, 2, 3
8	Trajectory	115%	4.1		1
9	Trajectory	100%	5.4		1
10	Trajectory	100%	6.8		1
11	Constant motor position	100%	N/A ^a		3

a. Peak BAM is not specified for motor position sinusoid and constant position (non-trajectory tracking) input conditions. Both inputs are defined as desired motor positions, a sinusoid of positions (condition 1) or constant position (condition 11). Motor positions are measured at the motor shaft with an encoder.

Conditions one and two were tested to evaluate performance specifications. The remaining conditions were tested to answer key questions one to three, i.e. to evaluate the effects of walking speed, peak BAM, and gait kinematics on trajectory tracking performance. For all conditions, input-output data were recorded at 200 Hz and outputs filtered using a zero lag 4th-order low-pass Butterworth filter with 20 Hz cutoff frequency.

4.1 *Bandwidth Performance Evaluation*

System bandwidth was evaluated by comparing inputs of sinusoidal motor position, measured at the shaft by the motor encoder, to BAM outputs, measured at the knee brace by the load cell, in

condition one. The testing was performed in the configuration of Figure 17 on a stationary human subject to capture soft tissue dynamics.

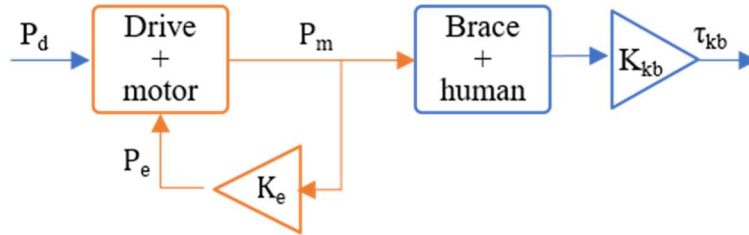


Figure 17. Control configuration for system frequency response characterization. Low-level PID control (orange) was run on the drive for position input tracking. Desired positions P_d are input to the motor drive, and tracked in a cascaded PID loop, depicted as the simplified feedback loop with encoder gain K_e and measured motor encoder position P_e . The actual motor position P_m is transmitted through the knee brace to the user, and the resulting knee brace BAM τ_{kb} measured with load cell K_{kb} .

Discrete sine frequencies of 1-12 Hz were evaluated with three repetitions per frequency. Bandwidth was defined as -3 dB roll off from the magnitude at the minimum tested 1 Hz frequency. Input amplitudes were adjusted to oscillate between 20 and 80% of a tolerable unloading level selected by the participant. The participant was instructed to bias weight toward the braced leg to better emulate soft tissue properties during single leg stance - the gait phase during which peak knee brace loading will occur.

The frequency response was extracted from the time domain signal using a fast Fourier transform (FFT): time series data of each discrete sine frequency input-output pair were separately transformed, averaged across trials, then compared to determine the magnitude ratio (output/input) and phase difference (output-input) between motor position input and BAM output.

4.2 *Peak BAM Performance Evaluation*

Knee brace peak BAM was evaluated in condition two, where a trajectory input with peak BAM of 8.1 Nm was used to challenge the system. Nominal walking speed was selected by the participant on an instrumented treadmill. The following trajectory parameters were held constant across all trajectory tracking trials: BAM rise to peak transition from 0 to 15 %GC, fall to minimum BAM transition from 60 to 75 %GC, and minimum BAM at 1.0 Nm from 75 to 100 %GC.

4.3 *Key Question Evaluation*

Trajectory tracking was evaluated for trajectories with 2.7-8.1 Nm peak BAM at $100 \pm 15\%$ patient selected walking speed (%WS) in conditions two through ten. RMS error was computed for each trajectory tracking condition.

Conditions five, seven, and eleven were compared to answer questions two and three, i.e. to characterize the effect of gait kinematics and soft tissue displacement due to muscle and leg volume changes during walking. Comparing tracking performance between standing (condition five) and walking (condition seven) will characterize the effect of the walking disturbance on tracking performance. Evaluating changes in BAM when a constant motor position is maintained will indicate whether kinematics and leg volume changes alone significantly affect the BAM. Taken together, these tests will inform us as to how much disturbance the controller is rejecting do to leg motion and leg volume changes.

During the stationary condition, the subject was instructed to bias weight toward the braced leg to better emulate soft tissue properties during single leg stance, and a 1 Hz gait cycle was emulated on the real-time controller with 60/40% ratio of stance to swing phase. In the constant motor position condition, the motor position was adjusted to yield knee brace BAM that

encompassed a 4.1 Nm peak BAM. Thirty to sixty steps were recorded for five conditions, and ten to thirty for the remaining five. These sample size categories are noted with results.

Chapter 5. RESULTS

ABLE was designed, developed, and tested on one healthy human participant. The system tracked a BAM trajectory over each gait cycle for a range of walking speeds and peak BAM magnitudes. Although no measures were tested for gait cycle estimation performance, the algorithm visibly detected heel strike events reliably, and adapted gait cycle durations to changes in gait frequency as intended with the Kalman filter based design. Results of individual tests are detailed below. No system failures (mechanical, electrical, nor software) were observed during human subject testing. All performance specifications were met, test results for each are summarized in Table 7. Results pertaining to key questions are detailed in §5.3 Key Question Evaluation.

Table 7. System performance specifications with results from associated test conditions.

Description	Specification	Actual	Test condition
Peak BAM	7 Nm	> 8 Nm	2
Bandwidth	10 Hz	≥ 12 Hz	1
Range of motion	120°	135°	

No human subject testing was performed to evaluate the brace range of motion specification. The actual range of motion is taken as the manufacturer specification (135°) as no modifications were made to the OTS brace that impact its range of motion.

5.1 *Bandwidth Performance Evaluation*

Frequency magnitude and phase are shown for the sampled motor position input BAM output pair in the Bode plot in Figure 18. Magnitude ranged from 51.6 to 52.5 dB and phase from -6 to 0 degrees for the tested 1 to 12 Hz input frequency range. The minimum magnitude was observed at 1 Hz, and the minimum phase at 12 Hz.

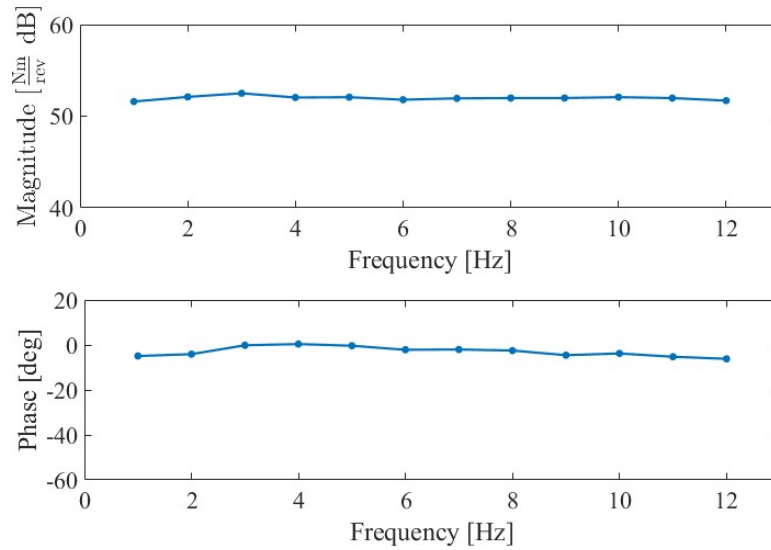


Figure 18. Bode plot for discrete sinusoidal 1-12 Hz motor position inputs to knee brace BAM output.

Both the magnitude and phase response are relatively flat, indicating a zero-order relationship between motor position input and BAM output within the evaluated 1-12 Hz region. As -3 dB roll off was not observed, the system bandwidth is not known, but is greater than the 10 Hz design specification.

5.2 Peak BAM Performance Evaluation

A Peak BAM of 8.7 Nm was observed in condition two. Tracking results are shown in Figure 19.

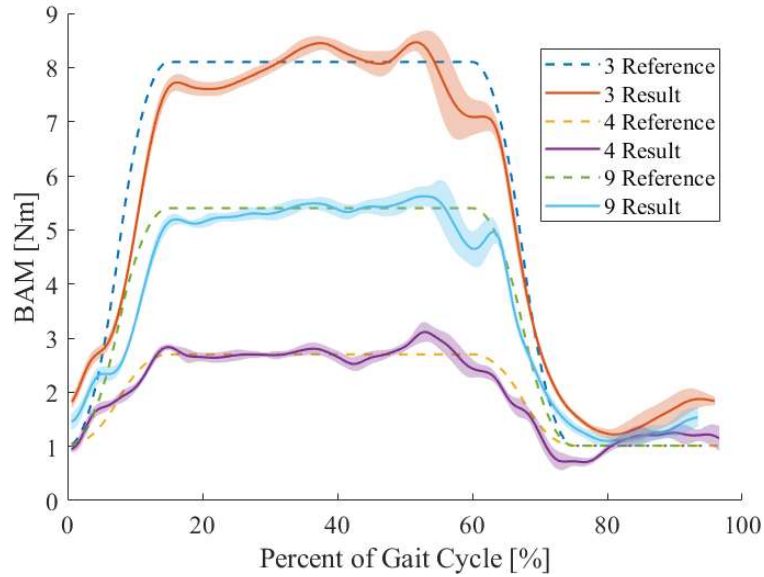


Figure 19. Select experimental conditions for comparison of Peak BAM magnitude and walking speed effect on trajectory tracking results. Condition 3 is 115 %WS 8.1 Nm peak BAM, 4 is 85 %WS with 2.7 Nm peak BAM, and 9 is 100 %WS with 5.4 Nm peak BAM. Lines are averages across steps and shaded regions are \pm one standard deviation.

5.3 Key Question Evaluation

Trajectory tracking results varied with walking speed and peak BAM magnitude. RMS error ranged from 0.18 to 0.58 Nm, with minimum observed at 100 %WS 4.1 Nm peak BAM (condition 7), and maximum at 115 %WS 8.1 Nm peak BAM (condition 3). The RMS error is listed for all trajectory tracking conditions in Table 8.

Table 8. Trajectory tracking RMS error results for conditions of varying walking speed and peak BAM magnitude.

Crossed cells indicate untested condition.

Walking Speed [m/s]	RMS error for Peak BAM [Nm]				
	2.7	4.1	5.4	6.8	8.1
1.1 (85 %WS)	0.19 ^a	0.23 ^a	/	/	/
1.3 (100 %WS)	/	0.18	0.36 ^a	0.49	0.56 ^a
1.5 (115 %WS)	/	0.30 ^a	/	/	0.58 ^a

a. Ten to thirty gait cycles recorded.

For key question one, the RMS error scaled with peak BAM, where an increase in peak BAM yielded an increase in RMS error. All three walking speeds (85 -115%) were only tested at the same peak BAM for one peak BAM level (4.1 Nm). Non-monotonic behavior resulted across walking speeds. Although it is not possible to draw meaningful conclusions on the relationship between walking speed and RMS error with the limited number of conditions tested, results indicate that variation in user walking speed affects tracking performance.

The contribution of gait kinematics to tracking performance (comparison of conditions five, seven, and eleven) is shown in Figure 20. For the constant motor position condition (no trajectory tracking), the average BAM ranged from 3.0 to 5.3 Nm. Comparing the walking and stationary trajectory tracking conditions, less BAM variation was observed for the stationary condition. During peak BAM (4.1 Nm desired for 15 to 60% gait cycle), the BAM range was 3.8 to 4.1 Nm for the stationary condition, and 3.6 to 4.2 Nm for the walking condition. Likewise, standard deviations ranged from 0.03 to 0.07 Nm and 0.09 to 0.27 Nm for stationary and walking conditions, respectively. Comparing standard deviations across the gait cycle, walking dynamics increase standard deviation (comparing Stationary TT to Walking CP conditions), and compensation decreases that variation (comparing Walking CP to Walking TT conditions).

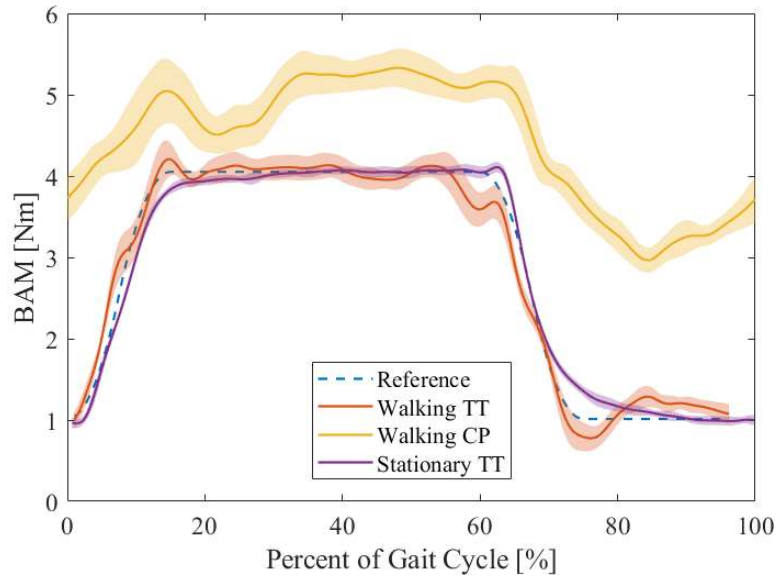


Figure 20. Experimental conditions for comparison of gait kinematic effects. Walking TT is trajectory tracking at 100 %WS 4.1 Nm peak BAM, Stationary TT is 4.1 Nm peak BAM while stationary, and Walking CP is 100 %WS with constant motor position. Lines are averages across steps and shaded regions are \pm one standard deviation.

For key question two, walking increased BAM standard deviation, and variation between actual and target BAM compared to the stationary trajectory tracking condition. For key question three, gait kinematics injected frontal plane disturbances, however they directionally drove load in the desired direction: BAM increased from 0-20% and decreased after 60% gait for the constant position condition. This relationship is also visible when comparing the walking and stationary trajectory tracking conditions. At the corners of the BAM trajectory (15%, 60%, and 75% gait cycle), the actual BAM outputs of each condition are on opposite sides of the target BAM curve, and the directional difference between them coincides with the BAM change of the walking constant position condition.

Chapter 6. DISCUSSION AND CONCLUSION

6.1 *Bandwidth Performance Evaluation*

The magnitude reflects the sensitivity of BAM to motor position, where $\sim 50\text{dB}$ corresponds to 400 Nm/rev. The gain amplifies motor positioning error. This relationship can be modified by the sheave (of the motor chassis) diameter: a decrease in sheave diameter theoretically yields a proportional decrease in gain. Considering that the range of speeds and BAMs required to carry out the trajectory are low relative to motor capability; the diameter could be minimized to mitigate motor positioning error effects on BAM output

6.2 *Key Question Evaluation*

Gait kinematics directionally drove load in the desired direction of BAM change. Comparing the constant motor position to trajectory tracking walking condition (seven and eleven), Modeling these dynamics could provide tracking and actuation performance benefits. The user's natural loading could be harnessed to reduce the actuation demands on an active brace, where a design could be optimized to mitigate energy consumption, actuator size, or accomplish the desired loading with passive, unpowered elements. This could be evaluated with an initial constant motor position phase where the periodic dynamics of the user are learned and incorporated into the feedforward scheme prior to trajectory tracking; such a model could also be implemented to improve tracking performance.

RMS error scaled with peak BAM, where error increased as peak BAM increased across conditions. Tracking performance was poorest at the transition from decreasing to minimum BAM, and at minimum BAM, encompassing 70 to 100 %GC. This could be a result of brace design, and/or feedback compensation performance. With respect to brace design, as the motor cannot

actively drive load in the negative direction, load reduction is governed by passive system compliance, namely the knee brace structure and human soft tissue. It follows that knee brace dynamics may be slowest near the minimum load state, i.e. as the knee brace relaxes from its loaded (peak BAM) state, it may be decelerating near the minimum load state, and may be less responsive to disturbances at the minimum load state. Comparing the stationary to walking trajectory tracking conditions of Figure 20, tracking performance is worse for the stationary condition during the transition from decreasing to minimum BAM (~70-80 %GC). Noting the coinciding decrease in BAM of the constant motor position condition from 70-80 %GC, it follows that tracking performance in the walking trajectory tracking condition may have been aided by the dynamics of the participants' gait. The system's capability to actively decrease load could be improved by incorporating a mechanism that stores energy while the knee brace is loaded, and releases it during unloading, e.g. with a spring and clutch. Addressing feedback compensation, tracking performance for minimum BAM values could be attributed to lack of controller response. In regions of the trajectory that are constant (during peak and minimum BAM), the feedforward path outputs a zero-velocity command by design, meaning all tracking is governed by the feedback path. Comparing tracking results across conditions in Figure 19, the difference between target and actual during minimum BAM (75-100 %GC) appears to scale from low to high walking speeds. Disturbance introduced by the subject's natural gait could scale with walking speed, thus placing higher demand on the feedback compensator to reduce tracking error. It follows that tracking error could be an interaction between the brace users' natural gait dynamics and an under tuned feedback compensator.

The RMS errors are considered adequate for system performance. Although we are unaware of a basis for specifying acceptable error from a clinical nor a biomechanical perspective,

there is certainly some error threshold from an investigation standpoint. We set out to design a system capable of yielding varying unloading trajectories at the knee brace. If these trajectories were to vary greatly with respect to the desired trajectory, then investigation of novel unloading profiles would not be possible. In this sense, the actual BAM varied from target in a range we deem adequate for the system's purpose of investigating the efficacy of unloading profiles for conservative medial KOA treatment.

6.3 *Conclusion*

In order to explore new robotic braces designs that address the shortcomings of current unloader braces, we developed and evaluated a novel robotic unloader brace with offboard actuation. The system was design and tested with one human subject. System performance was deemed adequate for subsequent future human subject laboratory gait studies. It is essential that tracking errors and engineering performance shortcomings are cast into a biomechanical domain, and their significance considered from a clinical perspective, e.g. the observed, less aggressive transition from maximum to minimum BAM could be desirable behavior from a user comfort perspective. The developed system is considered adequate for subsequent laboratory investigation where emulated passive brace (constant motor position) behavior is compared to active unloading profiles for biomechanical outcomes such as peak KAM and knee adduction angular impulse, and subjective measures of pain and comfort. At a high level, such studies are intended to guide how a brace could better interact with a user from a loading perspective. It should be noted that while we aimed to design a flexible system, ABLE is limited as a research tool. For example, braces can be bulky and obtrusive devices - investigation with ABLE will not address these shortcomings of brace efficacy. The value of ABLE is that it can turn load 'off', which invites questions about how, when, and why a brace should transition between these states, and what characteristics of those

transitions are and are not beneficial. Answers to such questions could give rise to a new class of unloader braces that adapt to diverse user loading conditions, improve patient compliance, and delay invasive, costly interventions common to the current KOA treatment paradigm.

BIBLIOGRAPHY

- [1] R. C. Lawrence *et al.*, “Estimates of the prevalence of arthritis and other rheumatic conditions in the United States. Part II,” *Arthritis Rheum.*, vol. 58, no. 1, pp. 26–35, 2008.
- [2] A. A. Guccione *et al.*, “The effects of specific medical conditions on the functional limitations of elders in the Framingham study,” *Am. J. Public Health*, vol. 84, no. 3, pp. 351–358, 1994.
- [3] M. R. Maly, P. A. Costigan, and S. J. Olney, “Mechanical factors relate to pain in knee osteoarthritis,” *Clin. Biomech.*, vol. 23, no. 6, pp. 796–805, 2008.
- [4] D. J. Hunter, T. Neogi, and M. C. Hochberg, “Quality of osteoarthritis management and the need for reform in the us,” *Arthritis Care Res.*, vol. 63, no. 1, pp. 31–38, 2011.
- [5] S. X. Wang, A. X. Ganguli, D. Macaulay, W. Reichmann, J. K. Medema, and M. A. Cifaldi, “The economic burden of osteoarthritis in Americans: analysis from a privately insured population,” *Osteoarthr. Cartil.*, vol. 22, no. 2014, p. S210, 2014.
- [6] E. Losina, “Cost-effectiveness of Total Knee Arthroplasty in the United States,” *Arch. Intern. Med.*, vol. 169, no. 12, pp. 1113–1121, 2009.
- [7] J. Ledingham, M. Regan, A. Jones, and M. Doherty, “Radiographic patterns and associations of knee osteoarthritis,” *Rheumatol. (United Kingdom)*, vol. 32, p. 140, 1993.
- [8] D. Zhao, S. A. Banks, K. H. Mitchell, D. D. D’Lima, C. W. Colwell, and B. J. Fregly, “Correlation between the Knee Adduction Torque and Medial Contact Force for a Variety of Gait Patterns,” *Anticancer Res.*, 1991.
- [9] J. P. Walter, D. D. D’Lima, C. W. Colwell, and B. J. Fregly, “Decreased knee adduction

- moment does not guarantee decreased medial contact force during gait,” *J. Orthop. Res.*, 2010.
- [10] D. E. Hurwitz, A. B. Ryals, J. P. Case, J. A. Block, and T. P. Andriacchi, “The knee adduction moment during gait in subjects with knee osteoarthritis is more closely correlated with static alignment than radiographic disease severity, toe out angle and pain,” *J. Orthop. Res.*, 2002.
- [11] M. Henriksen, M. W. Creaby, H. Lund, C. Juhl, and R. Christensen, “Is there a causal link between knee loading and knee osteoarthritis progression? A systematic review and meta-analysis of cohort studies and randomised trials,” *BMJ Open*. 2014.
- [12] P. Levinger, H. B. Menz, A. D. Morrow, J. A. Feller, J. R. Bartlett, and N. R. Bergman, “Foot kinematics in people with medial compartment knee osteoarthritis,” *Rheumatol. (United Kingdom)*, 2012.
- [13] K. D. Gross and H. J. Hillstrom, “Noninvasive Devices Targeting the Mechanics of Osteoarthritis,” *Rheum. Dis. Clin. North Am.*, vol. 34, no. 3, pp. 755–776, 2008.
- [14] T. Duivenvoorden *et al.*, “Duivenvoorden_et_al-2015-The_Cochrane_library.sup-2,” *The Cochrane*, no. 3, p. 54 pág., 2015.
- [15] E. Squyer, D. L. Stamper, D. T. Hamilton, J. A. Sabin, and S. S. Leopold, “Unloader knee braces for osteoarthritis: Do patients actually wear them?,” *Clin. Orthop. Relat. Res.*, vol. 471, no. 6, 2013.
- [16] R. D. A. Gaasbeek, B. E. Groen, B. Hampsink, R. J. van Heerwaarden, and J. Duysens, “Valgus bracing in patients with medial compartment osteoarthritis of the knee,” *Gait Posture*, vol. 26, no. 1, pp. 3–10, 2006.
- [17] U. Della Croce *et al.*, “A preliminary assessment of a novel pneumatic unloading knee

- brace on the gait mechanics of patients with knee osteoarthritis,” *PM R*, vol. 5, no. 10, pp. 816–824, 2013.
- [18] J. M. Caputo and S. H. Collins, “An experimental robotic testbed for accelerated development of ankle prostheses,” in *Proceedings - IEEE International Conference on Robotics and Automation*, 2013.
- [19] J. R. Koller, D. H. Gates, D. P. Ferris, and C. D. Remy, “Confidence in the curve: Establishing instantaneous cost mapping techniques using bilateral ankle exoskeletons,” *J. Appl. Physiol.*, 2016.
- [20] K. B. Heer, “Design and Control of a Lower-Limb Exoskeleton Emulator for Accelerated Development of Gait Exoskeletons,” Colorado School of Mines, United States -- Colorado, 2017, 2017.
- [21] C. H. Fantini Pagani, C. Bhle, W. Potthast, and G. P. Brggemann, “Short-term effects of a dedicated knee orthosis on knee adduction moment, pain, and function in patients with osteoarthritis,” *Arch. Phys. Med. Rehabil.*, vol. 91, no. 12, pp. 1936–1941, 2010.
- [22] T. Schmalz, E. Knopf, H. Drewitz, and S. Blumentritt, “Analysis of biomechanical effectiveness of valgus-inducing knee brace for osteoarthritis of knee,” *J. Rehabil. Res. Dev.*, vol. 47, no. 5, p. 419, 2010.
- [23] D. A. Winter, *Biomechanics and Motor Control of Human Movement: Fourth Edition*. 2009.
- [24] W. C. Young, *Roark’s Formulas for Stress & Strain: Fourth Edition*. 1989.
- [25] R. M. Murray, *Optimization-Based Control Control and Dynamical Systems*. 2009.

**APPENDIX A: CODE AND RESULTS FOR OFF-BOARD
SYSTEM MOTOR SPECIFICATION**

Contents

- §I. Declare inputs
- §II. Generate desired BAM profile/trajectory
- §V. Compute desired motor torque without kinematics, i.e. rigid system
- §VI. Add motor kinetics from kinematic trajectory
- §VII. Compute desired motor torque (dynamic) considering motor inertia
- §VIII. Plot

```
% Dylan Reinsdorf
% Rev 1.0

clc, clear all, close all

% PURPOSE
% This code computes the motor torque and speed trajectory for a desired
% BAM profile, i.e. it simulates a simplified dynamical model of the robotic
% brace system to compute the motor trajectory required to achieve a
% desired BAM trajectory at the knee brace within each gait cycle.

% DESCRIPTION

% To perform the simulation, assumptions on system input parameters e.g.
% brace stiffness (required to include motor acceleration) are made, and a
% safety factor used to account for their uncertainty. The safety factor
% also accounts for unmodeled dynamics such as Bowden cable friction, soft
% tissue compliance, and leg volume changes.

% Brace parameters are based on the Ottobock Agilum Reactive unloader
% brace, and BAM profile based on requirements specified as part of system
% design.
```

§I. Declare inputs

```
%For §II, BAM profile parameters:
    n = 1000; % samples in trajectory
    BAMpk = 8.1; %peak BAM [Nm]
    BAMmin = 1; %minimum BAM [Nm]
    risedur = 0.10; %BAM rise duration as percent of gait cycle [%]
    holddur = 0.55; %BAM hold (constant) duration as percent of gait cycle [%]
    rise0 = 0.05; %BAM rise start as percent of gait cycle [%]
    tstride = 1; %time per gait cycle [s]
%For §IV, compute motor kinematic trajectory:
    travel = 0.05; %linear pad and rope (1:1) travel required to reach peak BAM [m]
    sheaveOD = 1.5*0.0254; %Selected OD of sheave for off-board system (to be used with motor
    for which the trajectory is calculated in this script) [m]
    Kbrace = 3.6/travel; %brace stiffness from motor perspective, motor torque/linear brace t
    ravel [Nm/m], where 3.6Nm is the motor output required to reach peak BAM;
    Kbrace = Kbrace*pi*sheaveOD; %brace stiffness from rotational perspective, motor torque/m
    otor rotation [Nm/rev]
    Lb = 0.305; %Brace length [m]
```

```

Lc2c = 0.142; %Length/distance from shank strap center of pressure to condyle pad center
of pressure [m]
%For $VI, compute dynamic motor torque trajectory (incorporate angular
%accel):
    motorinertia = 6.22/10000*1.2; %motor inertia, scaled by 1.2 for added inertial component
s between motor and brace such as shaft coupler [kg*m^2]
    sf = 5; %safety factor to account for dynamic losses, e.g. friction, beyond those capture
d in transfer function.

```

§II. Generate desired BAM profile/trajectory

```

gc = 1:n; % vector of gait cycle points

%Create key points where curve changes behavior
p1 = round(rise0*n,0); %Initial duration @ BAMmin
p2 = round(risedur*n,0)+p1; %Rise to peak duration
p3 = round(holddur*n,0)+p2; %Hold @ peak duration
p4 = (p2-p1)+p3; %Fall to BAMmin duration
p5 = n; %Hold @ BAMmin duration (swing)

%Assign key points along gait cycle
iBAMprof = [[0 BAMmin];
            [p1 BAMmin];
            [p2 BAMpk];
            [p3 BAMpk];
            [p4 BAMmin];
            [p5 BAMmin]];

%Create curve using cubic interpolation to produce smooth curve
BAMprof = interp1(iBAMprof(:,1),iBAMprof(:,2),gc, 'PCHIP');

%Filter to smooth corners and therefore reduce acceleration and
%motor torque requirements
[B,A] = butter(4,60/1200/2);
BAMprof = filtfilt(B,A,BAMprof);

BAMprof = BAMprof'; %Transpose to organize data along columns

```

§V. Compute desired motor torque without kinematics, i.e. rigid system

```

Fcable = BAMprof/(Lc2c-Lc2c^2/Lb); % force required at cable at knee brace to yield desired B
AM [N]
motortrq = Fcable*sheaveOD/2; % torque required at motor shaft [Nm]

```

§VI. Add motor kinetics from kinematic trajectory

```

%Define gait cycle wrt time
dt = tstride/n; %time step [sec]
tgc = gc*dt; %gait cycle [sec]

%Motor deflection
motorpos = motortrq/Kbrace; %absolute position of motor at each instant of gait cycle [revs]

```

```

%Motor velocity
for i = 1:(length(tgc)-1)
    motorspeed(i) = (motorpos(i+1)-motorpos(i))/dt; %Motor velocity at each time point [r
ev/s]
end
motorspeed(i+1) = motorspeed(i);

%Motor acceleration
for i = 1:(length(tgc)-1)
    motoraccel(i) = (motorspeed(i+1)-motorspeed(i))/dt; %Motor velocity at each time poin
t [rev/s^2]
end
motoraccel(i+1) = motoraccel(i);
motoraccel = motoraccel*2*pi; %convert motor acceleration to rad [rad/sec^2]

```

§VII. Compute desired motor torque (dynamic) considering motor inertia

```

%Compute dynamic motor torque trajectory
for i = 1:length(tgc)
    motortrqtraj(i) = sf*(motoraccel(i)*motorinertia+motortrq(i));
end

%Print results to command window
disp('For the following input parameters:')
disp(['Time per stride = ', num2str(tstride), ' sec'])
disp(['Sheave/pulley OD = ', num2str(sheaveOD/0.0254), ' in'])
disp(['Motor inertia = ', num2str(motorinertia), ' kg*m^2'])
disp(['Safety factor = ', num2str(sf)])
disp(' ')
disp('A motor with the following specifications will be sufficient for tracking the desir
ed BAM profile:')
disp(['Continuous torque >= ', num2str(mean(abs(motortrqtraj))), ' Nm'])
disp(['Speed >= ', num2str(max(abs(motorspeed*60))), ' rpm'])
disp(['Peak torque >= ', num2str(max(abs(motortrqtraj))), ' Nm'])

```

For the following input parameters:

Time per stride = 1 sec
 Sheave/pulley OD = 1.5 in
 Motor inertia = 0.0007464 kg*m²
 Safety factor = 5

A motor with the following specifications will be sufficient for tracking the desired BAM profile:

Continuous torque >= 7.0476 Nm
 Speed >= 189.0422 rpm
 Peak torque >= 10.3244 Nm

§VIII. Plot

```

%Desired BAM profile with seed points
figure()
plot(iBAMprof(:,1)/n,iBAMprof(:,2),'o')
hold on

```

```

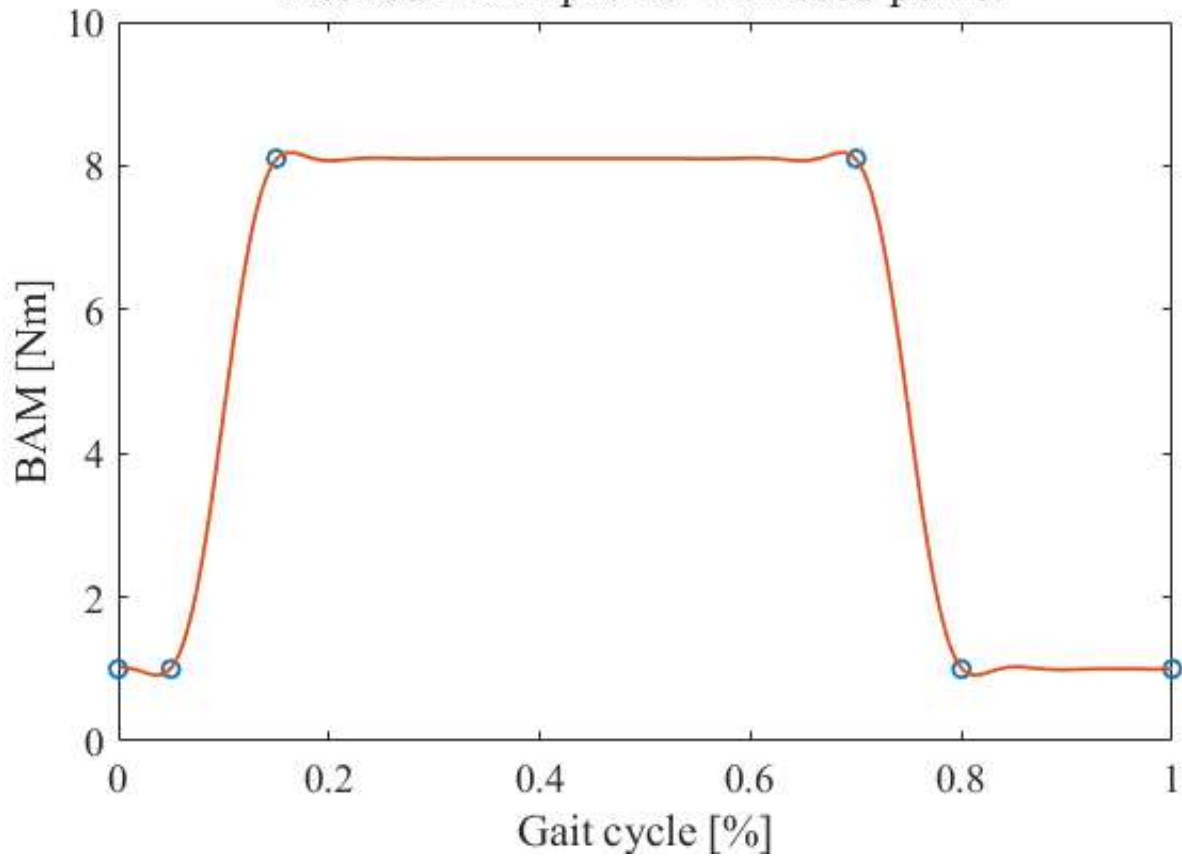
plot(gc/n,BAMprof)
xlabel('Gait cycle [%]')
ylabel('BAM [Nm]')
title('Desired BAM profile with seed points', 'Interpreter', 'latex')
figReportFormat(gcf,[1.3,-1,14])

%Motor trajectory
figure()
plot(motorspeed*60,motortrqtraj);
hold on
plot(mean(abs(motorspeed*60)),mean(abs(motortrqtraj)), 'x')
title('Motor trajectory', 'Interpreter', 'latex')
xlabel('Motor velocity [rpm]')
ylabel('Motor torque [Nm]')
legend('Motor trajectory', 'Mean', 'Location', 'southeast')
figReportFormat(gcf,[1.3,-1,14])

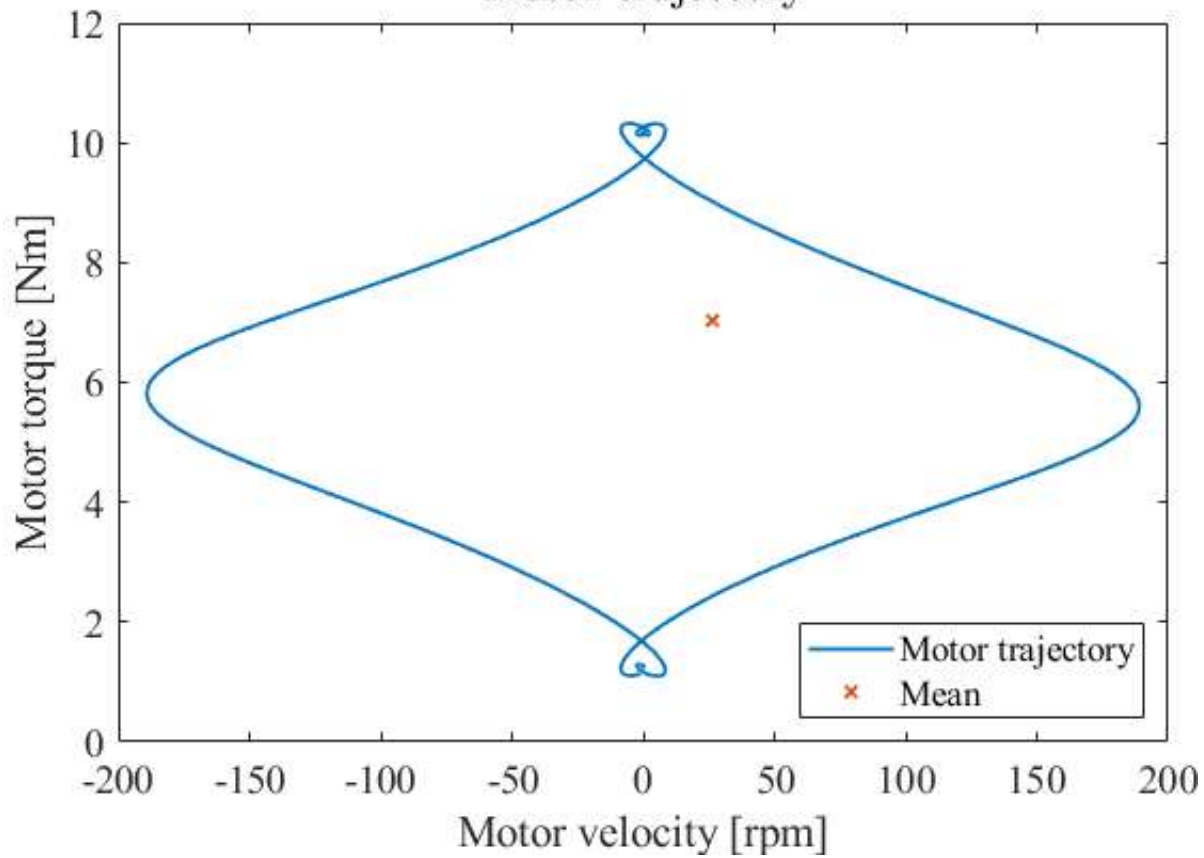
figure()
% Desired torque and angular acceleration
plot(tgc,motoraccel)
ylabel('Acceleration [rad/sec^2]')
yyaxis right
plot(tgc,motortrq)
ylabel('Motor Torque [Nm]')
xlabel('Gait cycle [sec]')
title('Desired torque ( $\tau_d$ ) and angular acceleration ( $\ddot{\theta}_d$ )', 'Interpreter', 'latex')
legend({' $\ddot{\theta}_d$  \ [rad/sec^2]', ' $\tau_d$  [Nm]'}, 'Interpreter', 'latex', 'Location', 'south')
figReportFormat(gcf,[1.3,-1,14])

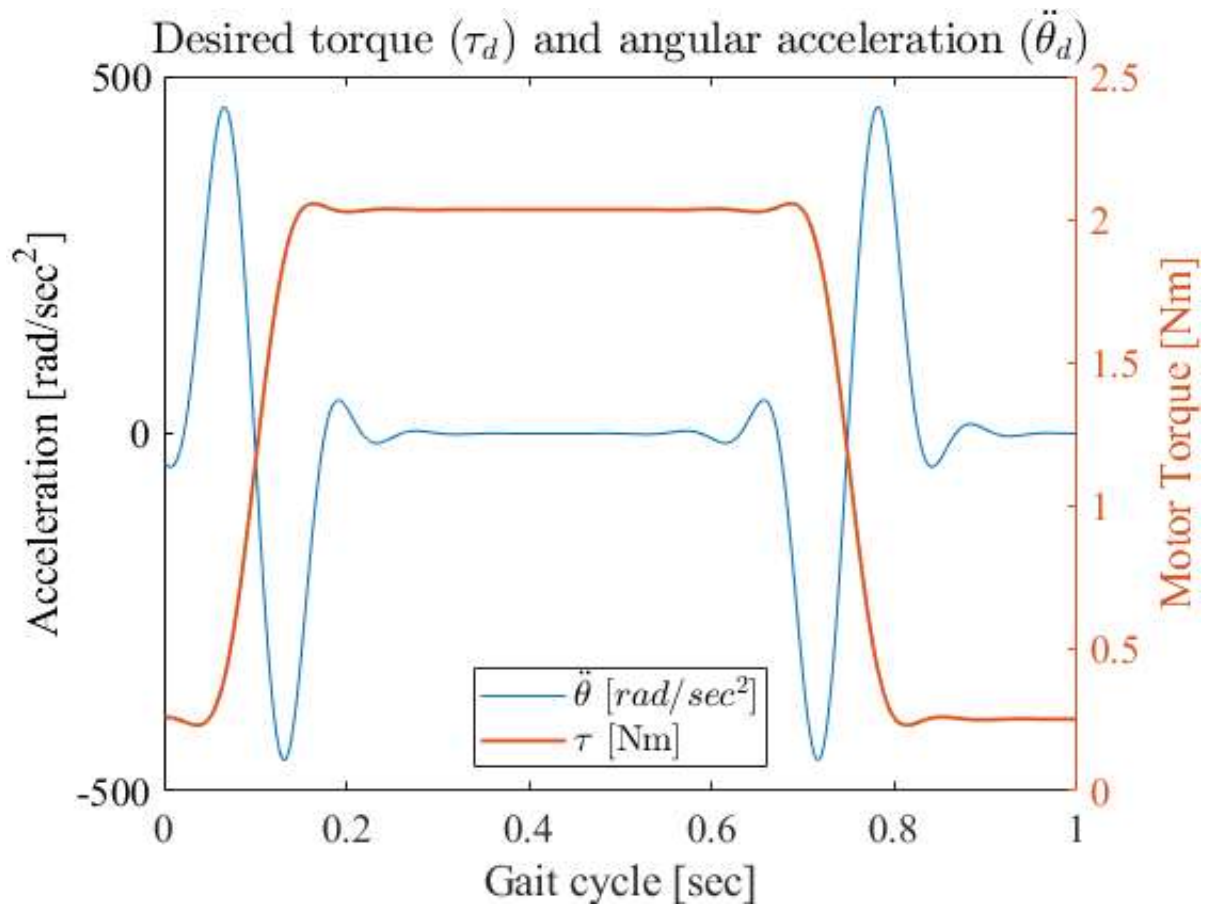
```

Desired BAM profile with seed points



Motor trajectory





APPENDIX B: MOTOR TRANSMISSION ANALYSIS AND DESIGN

Shaft Specification for ABLE Transmission

Purpose

This code is intended to assist specification of a D-profile shaft using stress analysis. Torque is generated by a motor mated to the shaft via a flexible shaft coupling.

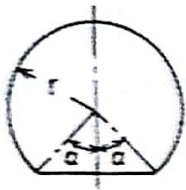
Background

The shaft is coupled to a Kollmorgen AKM-52H motor. It is supported by a mounted bearing at both ends.

Description

Torsional stress will be calculated using formulae for a D-profile cross section from Roark's Formulas for Stress and Strain 8th Ed, pictured below:

7. Circular segmental section



[Note: $h = r(1 - \cos \alpha)$]

$K = 2Cr^4$ where C varies with $\frac{h}{r}$ as follows:

For $0 \leq \frac{h}{r} \leq 1.0$,

$$C = 0.7854 - 0.0333 \frac{h}{r} - 2.6183 \left(\frac{h}{r} \right)^2 \\ + 4.1595 \left(\frac{h}{r} \right)^3 - 3.0769 \left(\frac{h}{r} \right)^4 \\ + 0.9299 \left(\frac{h}{r} \right)^5$$

$\tau_{\max} = \frac{TB}{r^3}$ where B varies with $\frac{h}{r}$ as follows:

For $0 \leq \frac{h}{r} \leq 1.0$,

$$B = 0.6366 + 1.7598 \frac{h}{r} - 5.4897 \left(\frac{h}{r}\right)^2 + 14.062 \left(\frac{h}{r}\right)^3 - 14.510 \left(\frac{h}{r}\right)^4 + 6.434 \left(\frac{h}{r}\right)^5$$

(Date from Refs. 12 and 13)

The form of B is a Taylor series, with terms greater than order=5 neglected. The maximum shear stress from the torsionally loaded shaft will be computed for multiple D-profile shaft sizes, followed by bending stress for a central load. Stresses are combined into a principle stress and safety margins computed for each. Shaft dimensions from McMaster Carr are used.

Note: nominal shaft sizes are used for calculations.

Declare Inputs

```
T = 191; % peak torque of AKM-52H [lb-in]
tauy = 35*1000; % yield strength of SS303 [psi]
r = [0.375 0.5 0.625 0.75 1]/2; % shaft radius
dflat = r; % width of the flat portion of the shaft cross section [in].
Dshv = 1; % assumed sheave diameter [in]
l = 3; % length between bearings, the effective length used to find max bending moment
```

Shaft geometry

Compute the variables related to shaft geometry required per the equations of §Description.

```
alpha = asind(dflat/2./r); % [degrees]
h = r.*(1-cosd(alpha)); % [in]
B = 0.6366+1.7598*h./r...
    -5.4891*(h./r).^2+14.062*(h./r).^3 ...
    -14.510*(h./r).^4+6.434*(h./r).^5; % by the form of this equation
```

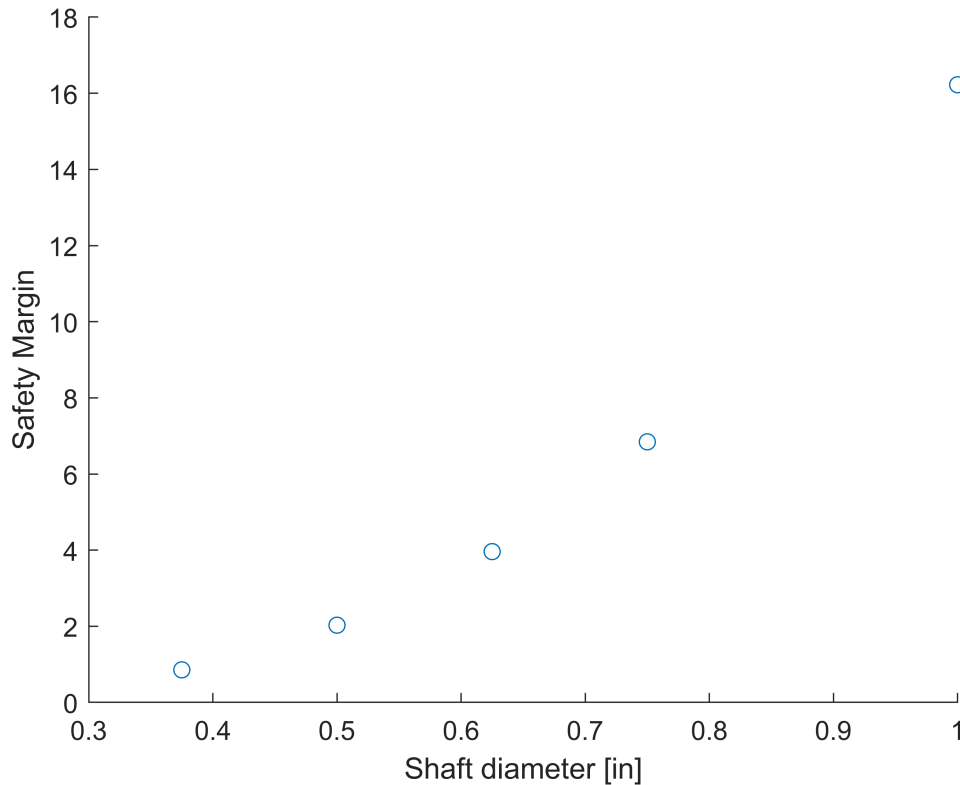
Maximum stress

```
taumax = T*B./r.^3; % max shaft stress torsion [psi]
I = pi*r.^4/4; % second moment of inertia for a circular cross section (worst case over D prof:
Mmax = T/Dshv*l/4; % max bending moment at center of shaft
sigmax = Mmax*r./I; % maximum bending stress [psi]
sigp = 0.5*(sigmax+sqrt(sigmax.^2+4*taumax.^2)); % principle stress
SM = tauy./sigp % safety factor [dimensionless]
```

```
SM = 1x5
    0.8555    2.0279    3.9607    6.8441    16.2232
```

```
figure() % plot result
```

```
scatter(r*2,SM)
ylabel('Safety Margin')
xlabel('Shaft diameter [in]')
```



Moment of inertia comparison

This computation is performed for a circular cross section.

```
rho = 8/1000; % density of SS303 [kg/cm^3]
L = 3.5*2.54; % shaft length [cm]
M = pi*(r*2.54).^2*L*rho; % mass of shaft [kg]
Ishaft = 0.5*M.*(r*2.54).^2 % moment of inertia about axis of rotation [lbf*in^2] (worst case a
```

```
Ishaft = 1x5
    0.0057    0.0182    0.0443    0.0920    0.2906
```

```
Imotor = 6.22; % inertia of motor [kg*cm^2]
((Ishaft+Imotor)./Imotor-1)*100 % increase in moment of inertia [%]
```

```
ans = 1x5
    0.0924    0.2920    0.7129    1.4784    4.6724
```

Motor Frame Specification for ABLE transmission

Purpose

This code is intended to assist specification of the motor frame using stress and thermal analysis.

Background

Forces are transmitted to the frame via motor generated torques. The motor, a Kollmorgen AKM-52H, is flange mounted to the mounting plate. Frame is configured as a two walled shear box, a rectangular prism with 5 side. The motor is located at the top face of the prism, and the shaft and bearings fixed to one of the vertical sides. The remaining sides are included for torsional stiffness.

Description

To select motor plate material, thermal analysis is performed to determine change in size of the motor plate for temperature rise. Aluminum is preferred for a machinability, cost, and weight perspective, however exhibits less dimensional stability over temperature change.

To select fastener quantities used to fix the vertical walls of the frame to the top and base, shear stress analysis is used. 3/8" thickness Al plate has been selected for the motor and vertical wall due to design geometric constraints and engineering acumen. 10-32 fasteners will be used to mate this vertical wall to the top and base plates. 1/4" thickness Al plate has been selected for the base and additional vertical wall to decrease mass and cost. The thickness of these plates is not further decreased to allow for tapping of 6-32 holes along the 1/4" width faces of the vertical plate, and counterboring on the base plate. The quantity of 10-32 and 6-32 fasteners will be selected based on stress analysis.

```
clear all, clc
```

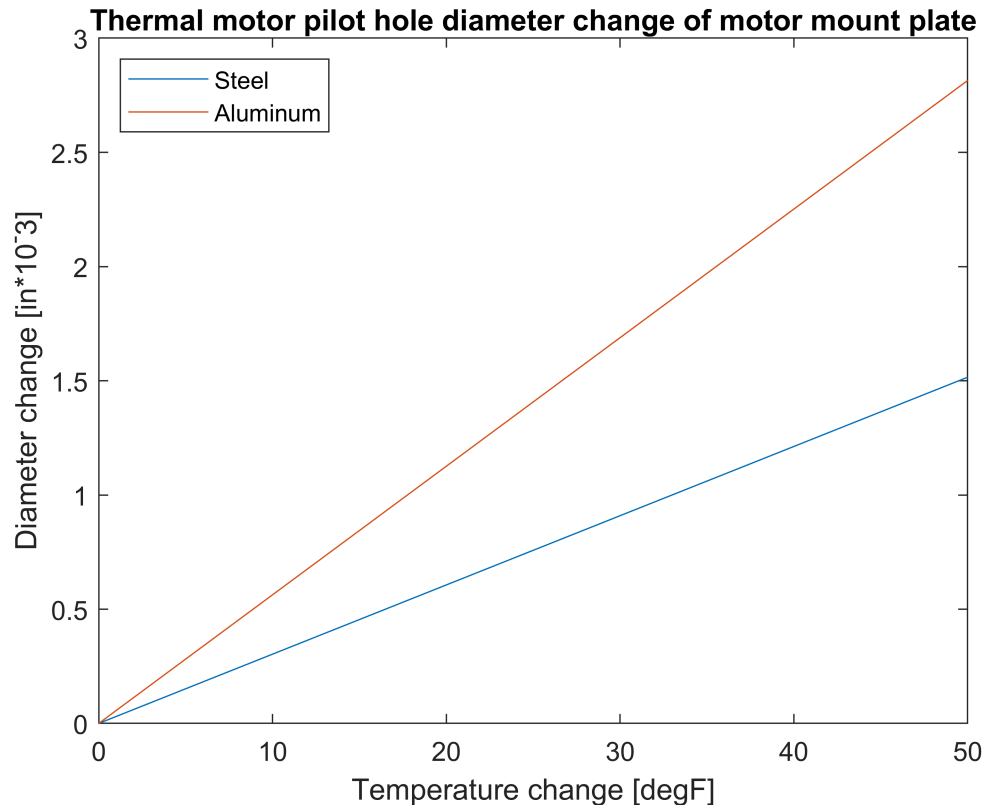
Thermal Analysis for Motor Plate

Analysis if performed for Al 6061 and low carbon steel.

```
%Declare inputs
deltaT = 0:5:50; % temp change [degF]
r = 4.33/2 ; % [in]
% Steel
alphaFe = 7*10^-6; % coefficient of linear expansion for steel[in/in/degF]
deltaDFe = r*deltaT.*alphaFe*2; % diameter change [in]
% Aluminum
alphaAl = 13*10^-6; % coefficient of linear expansion for steel[in/in/degF]
deltaDA1 = r*deltaT.*alphaAl*2; % diameter change [in]

figure()
plot(deltaT,deltaDFe*1000,deltaT,deltaDA1*1000)
xlabel('Temperature change [degF]')
ylabel('Diameter change [in*10^-3]')
title('Thermal motor pilot hole diameter change of motor mount plate')
```

```
legend('Steel', 'Aluminum', 'Location', 'Northwest')
```



Stress Analysis for Fasteners

The fasteners are positioned along vertical and horizontal lines. The worst case shear load at each bolt is where the distance from the motor is shortest, yielding the highest force generated from the motor torque. To simplify analysis, the minimum distance from the motor shaft center of rotation will be used, 1.6875". This, in effect, is assuming the fasteners are distributed at an equal radius around the motor, which is worst case and therefore acceptable.

Shear stress is calculated as $\tau = \frac{4V}{3A}$, where V is the force, and A the area corresponding to the minor diameter of the fastener.

```
%Declare inputs
T = 191; % peak torque of AKM-52H [lb-in]
tauy = 30*1000; % yield strength of SS 18-8 [psi]
A = [0.00874, 0.0175]; % area of [6-32 10-32] fastener, from Machinery's Handbook 28th Ed. [in^2]
r = 1.6875; % minimum distance of motor shaft (torque) center to fastener center [in]
qty = [2 3 4 5 6]; % fastener quantity

%Compute stress in single fastener
tau(1) = (4*T/r)/(3*A(1)); % shear stress for 6-32
tau(2) = (4*T/r)/(3*A(2)); % shear stress for 10-32

%Compute safety factor for all quantity permutations
for i1 = 1:length(qty) % outer loop for 10-32 qty
```

```

for i2 = 1:length(qty) % inner loop for 6-32 qty
    FS(i1,i2) = (tau(1)*qty(i1)+tau(2)*qty(i2))/tauy; % compute safety factor
end
end

%Display results
FStable = table(FS(:,1), FS(:,2), FS(:,3), FS(:,4), FS(:,5));
FStable.Properties.RowNames = {'Qty10_2' 'Qty10_3' 'Qty10_4' 'Qty10_5' 'Qty10_6'} ;
FStable.Properties.VariableNames = {'Qty6_2' 'Qty6_3' 'Qty6_4' 'Qty6_5' 'Qty6_6'};
FStable.Properties.Description = 'Factors of safety for quantities of 10-32 (rows) and 6-32 (columns) screws.';
FStable.Properties.Description;

```

```

ans =
'Factors of safety for quantities of 10-32 (rows) and 6-32 (columns) screws.'

```

```
FStable(:, :)
```

```
ans = 5x5 table
```

	Qty6_2	Qty6_3	Qty6_4	Qty6_5	Qty6_6
1 Qty10_2	1.7260	2.0135	2.3010	2.5884	2.8759
2 Qty10_3	2.3016	2.5891	2.8765	3.1640	3.4514
3 Qty10_4	2.8772	3.1646	3.4521	3.7395	4.0270
4 Qty10_5	3.4527	3.7402	4.0277	4.3151	4.6026
5 Qty10_6	4.0283	4.3158	4.6032	4.8907	5.1781

4

3

2

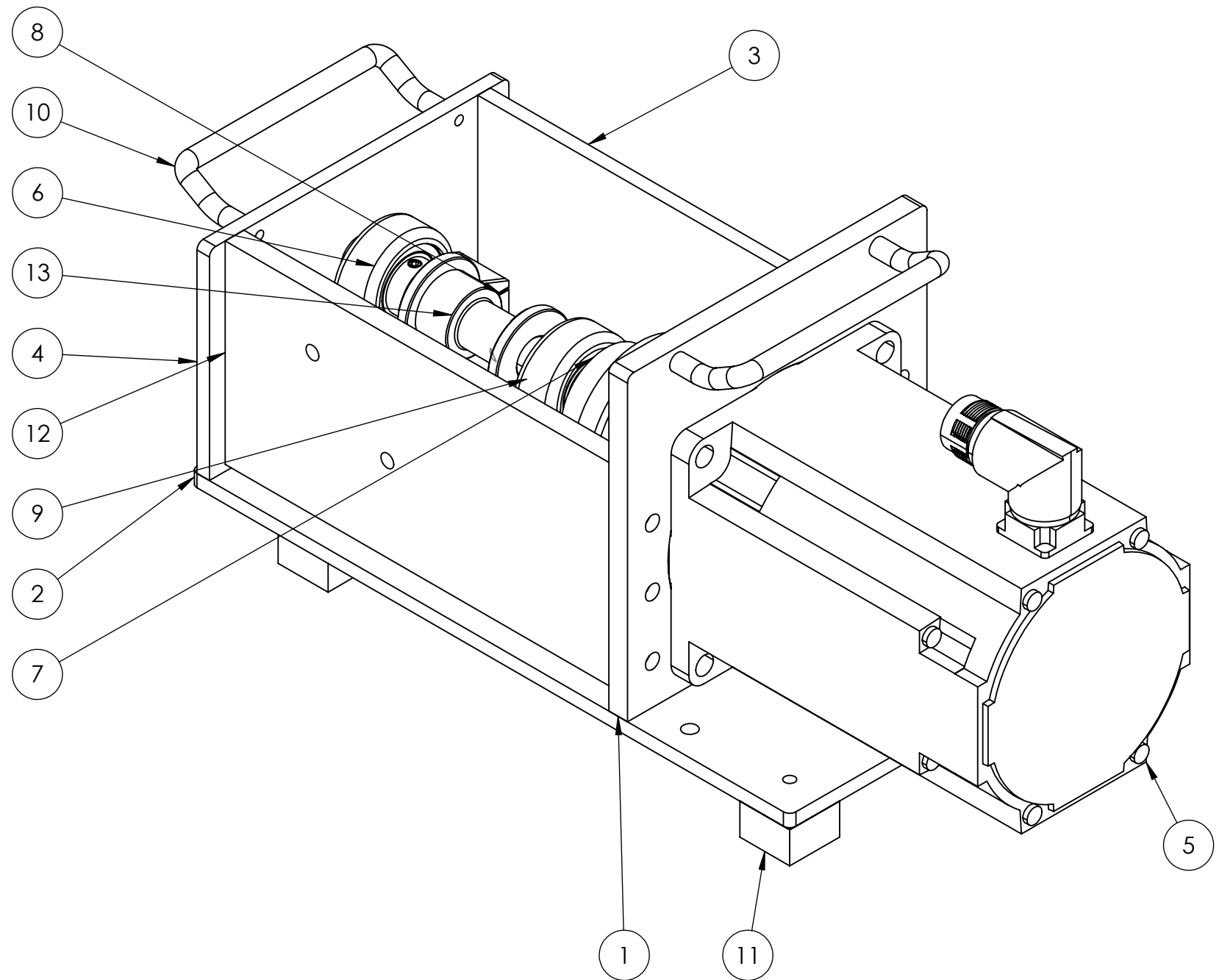
1

REV	CHANGE DESCRIPTION
1.0	INITIAL REVISION.
2.0	CHANGE FRAME FROM 80/20 TO MACHINED ALUMINUM PLATE.
2.1	REMOVE COUNTERBORES, REMOVE SECONDARY BASE PLATE.
2.2	UPDATE BOWDEN TERMINATION PLATE DESIGN PER MANUFACTURING PROCESS CHANGE FROM 3D PRINTED TO MACHINED.

INSPECTION:

- INSPECT CIRCLED DIMENSIONS

ITEM NO.	PART NUMBER	DESCRIPTION/SUPPLIER	QTY.
1	Motor mount plate	CUSTOM MACHINED COMPONENT	1
2	Bearing mount plate	CUSTOM MACHINED COMPONENT	1
3	Shear wall plate	CUSTOM MACHINED COMPONENT	1
4	Base plate	CUSTOM MACHINED COMPONENT	1
5	AKM52X_ANDNCA00	KAMAN AUTOMATION	1
6	2353K31	MOUNTED BEARING, MCMaster CARR	2
7	SC060R SHAFT COUPLING	KAMAN AUTOMATION	1
8	Bearing riser	CUSTOM MACHINED COMPONENT	2
9	8632T147	SHAFT CUT TO LENGTH = 5.50", MCMaster CARR	1
10	5245A6	HANDLE, MCMaster CARR	2
11	9306K821	FOOT, MCMaster CARR	4
12	Bowden termination plate	CUSTOM MACHINED COMPONENT	1
13	Cable Sheave - 3D print step shaft 0.010	CUSTOM 3D PRINTED COMPONENT	1



PROPRIETARY AND CONFIDENTIAL

THE INFORMATION CONTAINED IN THIS DRAWING IS THE SOLE PROPERTY OF VA PUGET SOUND RR&D CENTER FOR LIMB LOSS AND MOBILITY (CLIMB). ANY REPRODUCTION IN PART OR AS A WHOLE WITHOUT THE WRITTEN PERMISSION OF CLIMB IS PROHIBITED.

INSPECT CRITICAL DIMENSIONS, SEE SHEET 1

MATERIAL SPECIFIED IN NOTES OF EACH SHEET

SEE SHEET 1 FOR REVISION HISTORY

UNLESS OTHERWISE SPECIFIED:

DIMENSIONS ARE IN INCHES
TOLERANCES:TWO PLACE DECIMAL ± 0.005
THREE PLACE DECIMAL ± 0.003 INTERPRET GD&T PER:
ASME Y14.1-2009

DO NOT SCALE DRAWING

CLIMB
Center for Limb Loss and MoBility

NAME DATE

DRAWN D. REINSORF 1 OCT 18

CHECKED

TITLE:

KNEE BRACE MOTOR
CHASSIS

SIZE DWG. NO.

B

SCALE: 1:2 WEIGHT:

REV

2.2

SHEET 1 OF 7

4

3

2

1

B

A

4

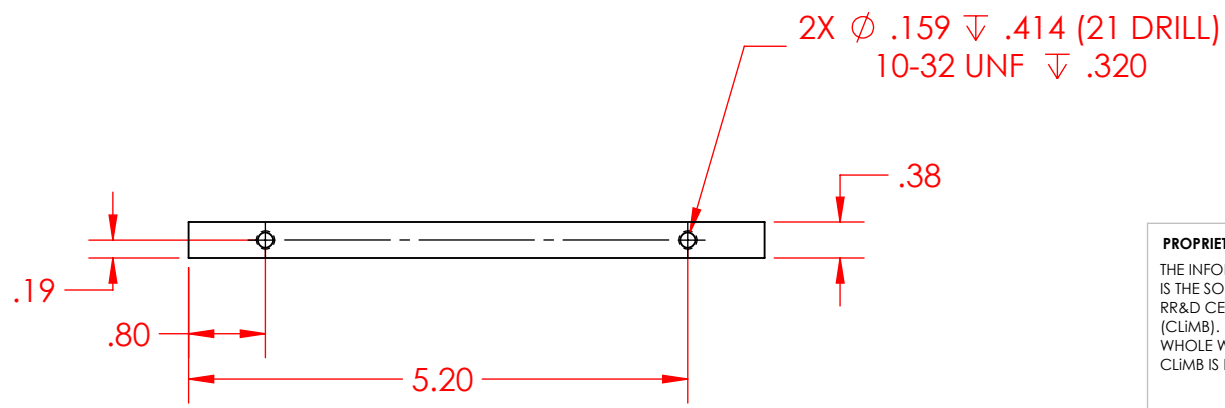
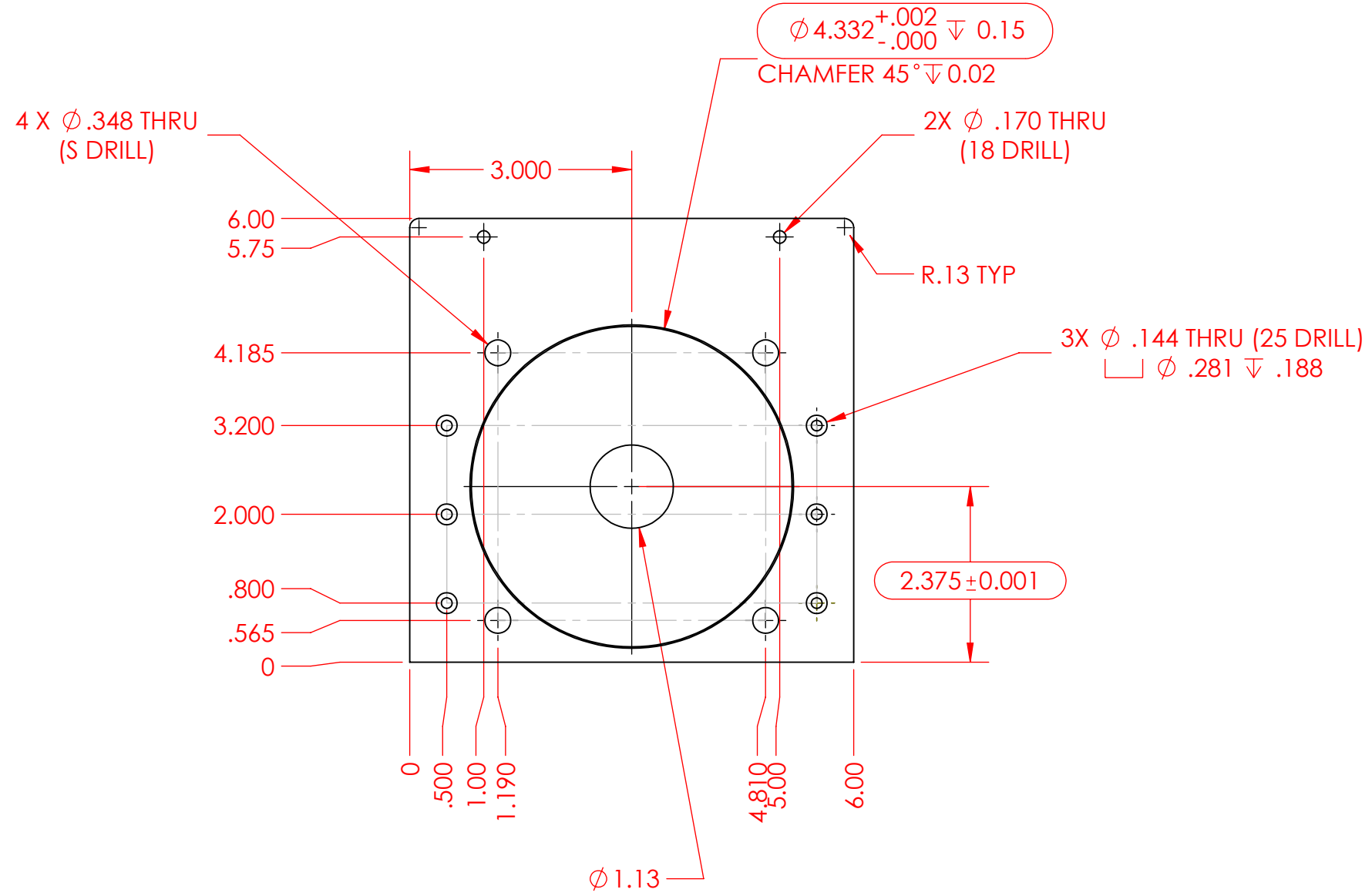
3

2

1

NOTES:

- BOM ITEM 1: MOTOR MOUNT PLATE
- MATERIAL: Al 6061



<p>PROPRIETARY AND CONFIDENTIAL</p> <p>THE INFORMATION CONTAINED IN THIS DRAWING IS THE SOLE PROPERTY OF VA PUGET SOUND RR&D CENTER FOR LIMB LOSS AND MOBILITY (CLIMB). ANY REPRODUCTION IN PART OR AS A WHOLE WITHOUT THE WRITTEN PERMISSION OF CLIMB IS PROHIBITED.</p>	<p>UNLESS OTHERWISE SPECIFIED:</p> <p>DIMENSIONS ARE IN INCHES</p> <p>TOLERANCES:</p> <p>TWO PLACE DECIMAL ± 0.005</p> <p>THREE PLACE DECIMAL ± 0.003</p>		<p>TITLE:</p> <p>KNEE BRACE MOTOR CHASSIS</p>				
	<p>INSPECT CRITICAL DIMENSIONS, SEE SHEET 1</p>		<p>INTERPRET GD&T PER:</p> <p>ASME Y14.1-2009</p>	<p>NAME</p> <p>D. REINSDORF</p>	<p>DATE</p> <p>1 OCT 18</p>	<p>SIZE</p> <p>B</p>	<p>DWG. NO.</p>
	<p>MATERIAL SPECIFIED IN NOTES OF EACH SHEET</p>	<p>DO NOT SCALE DRAWING</p>	<p>CHECKED</p>	<p>SCALE: 1:2</p>	<p>WEIGHT:</p>	<p>SHEET 2 OF 7</p>	

4

3

2

1

B

B

A

A

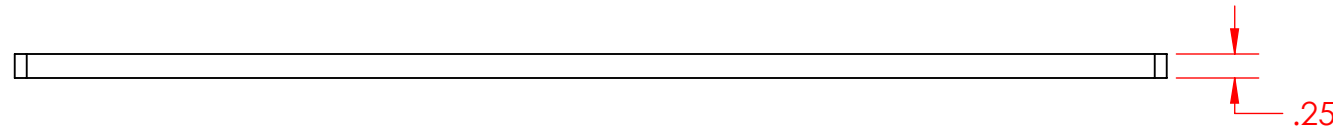
4

3

2

1

- NOTES:
- BOM ITEM 2: BEARING MOUNT PLATE
 - MATERIAL: Al 6061



4 X ϕ .323 THRU
(P DRILL)

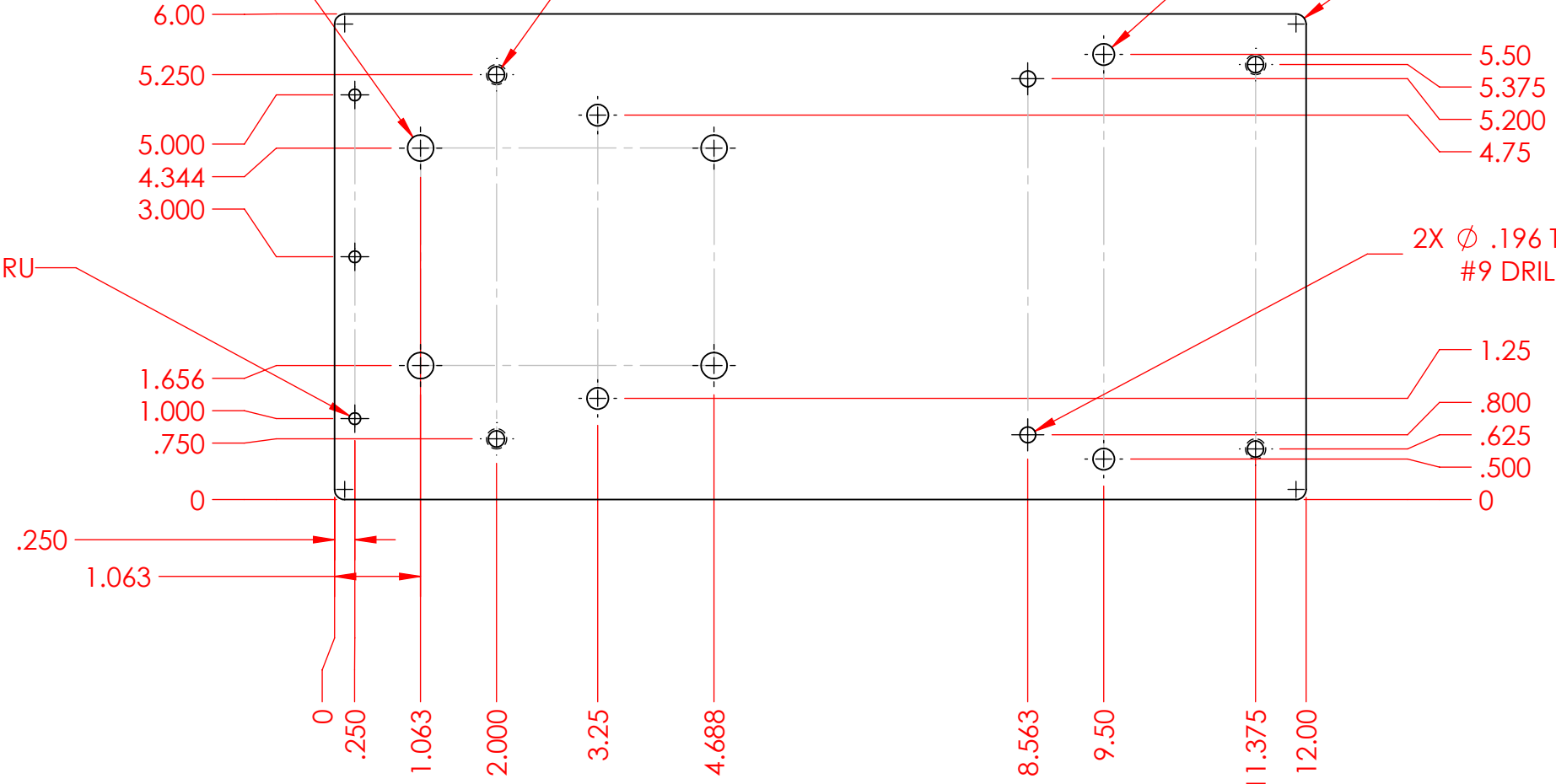
4X ϕ .201 THRU
1/4-20 UNC THRU

4X ϕ .266 THRU
(H DRILL)

R.13 TYP

3X ϕ .144 THRU

2X ϕ .196 THRU
#9 DRILL



<p>PROPRIETARY AND CONFIDENTIAL</p> <p>THE INFORMATION CONTAINED IN THIS DRAWING IS THE SOLE PROPERTY OF VA PUGET SOUND RR&D CENTER FOR LIMB LOSS AND MOBILITY (CLIMB). ANY REPRODUCTION IN PART OR AS A WHOLE WITHOUT THE WRITTEN PERMISSION OF CLIMB IS PROHIBITED.</p>	UNLESS OTHERWISE SPECIFIED:	 <p>Center for Limb Loss and Mobility</p>	TITLE:	
	DIMENSIONS ARE IN INCHES TOLERANCES:		KNEE BRACE MOTOR CHASSIS	
	TWO PLACE DECIMAL \pm 0.005 THREE PLACE DECIMAL \pm 0.003		SIZE	DWG. NO.
INSPECT CRITICAL DIMENSIONS, SEE SHEET 1	INTERPRET GD&T PER:	NAME	DATE	B
MATERIAL SPECIFIED IN NOTES OF EACH SHEET	ASME Y14.1-2009	DRAWN	D. REINSDORF	1 OCT 18
SEE SHEET 1 FOR REVISION HISTORY	DO NOT SCALE DRAWING	CHECKED		
			SCALE: 1:2	WEIGHT:
				SHEET 3 OF 7

4

3

2

1

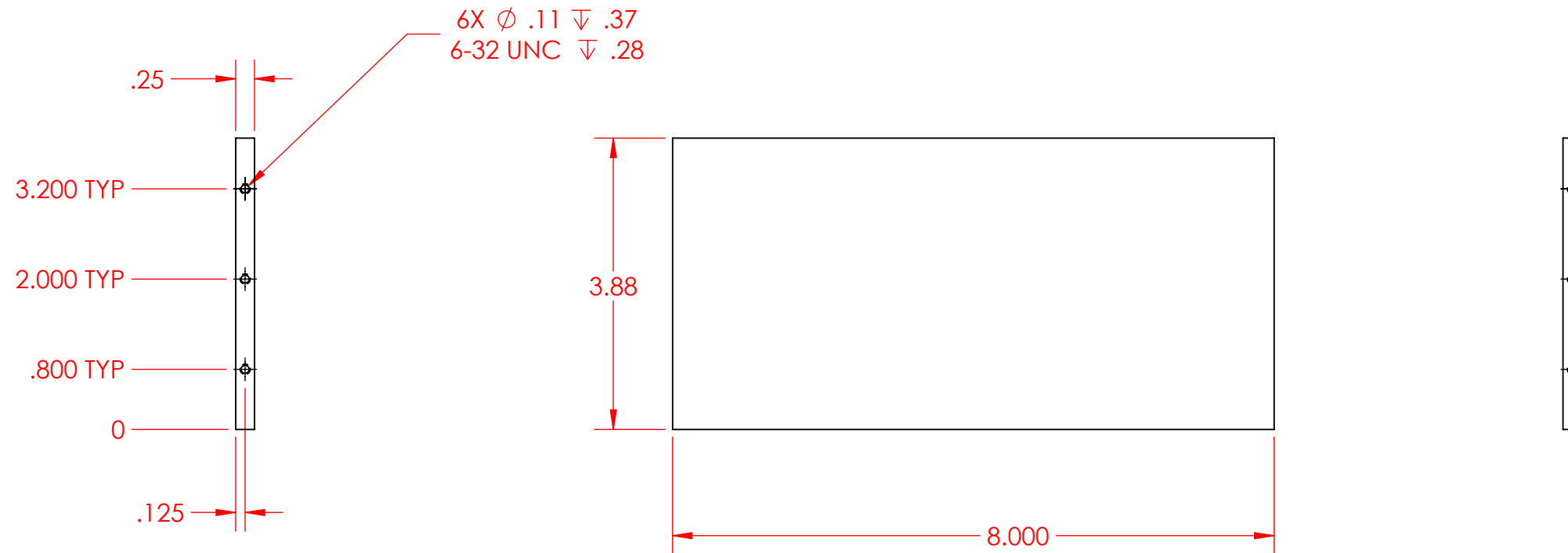
4

3

2

1

- NOTES:
- BOM ITEM 3: SHEAR WALL PLATE
 - MATERIAL: Al 6061



PROPRIETARY AND CONFIDENTIAL THE INFORMATION CONTAINED IN THIS DRAWING IS THE SOLE PROPERTY OF VA PUGET SOUND RR&D CENTER FOR LIMB LOSS AND MOBILITY (CLIMB). ANY REPRODUCTION IN PART OR AS A WHOLE WITHOUT THE WRITTEN PERMISSION OF CLIMB IS PROHIBITED.	UNLESS OTHERWISE SPECIFIED: DIMENSIONS ARE IN INCHES TOLERANCES: TWO PLACE DECIMAL ± 0.005 THREE PLACE DECIMAL ± 0.003	 Center for Limb Loss and MoBility	TITLE: KNEE BRACE MOTOR CHASSIS			
	INSPECT CRITICAL DIMENSIONS, SEE SHEET 1 MATERIAL SPECIFIED IN NOTES OF EACH SHEET SEE SHEET 1 FOR REVISION HISTORY		INTERPRET GD&T PER: ASME Y14.1-2009 DO NOT SCALE DRAWING	NAME D. REINS DORF	DATE 1 OCT 18	SIZE B
			SCALE: 1:2	WEIGHT:	SHEET 4 OF 7	

4

3

2

1

B

B

A

A

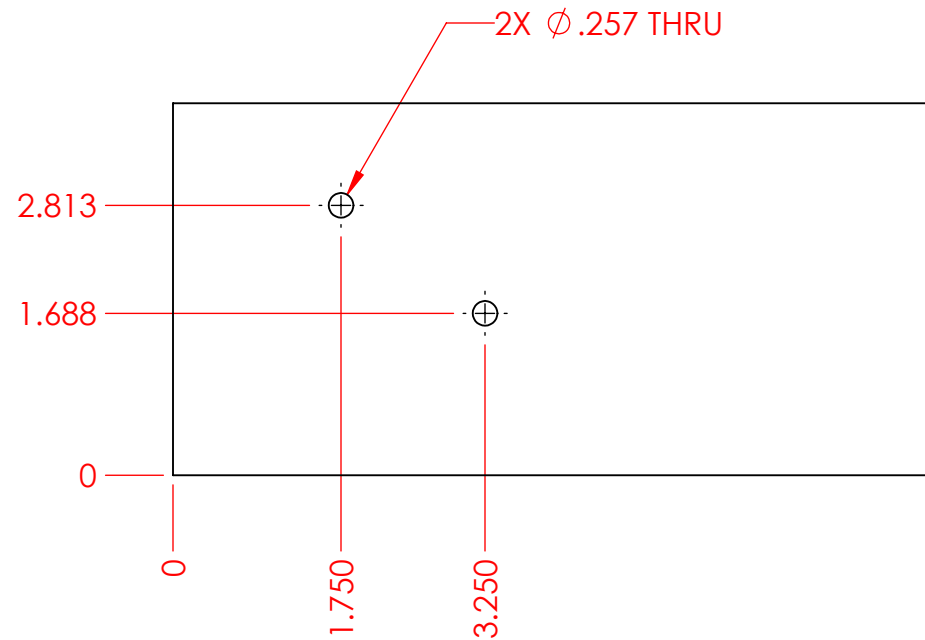
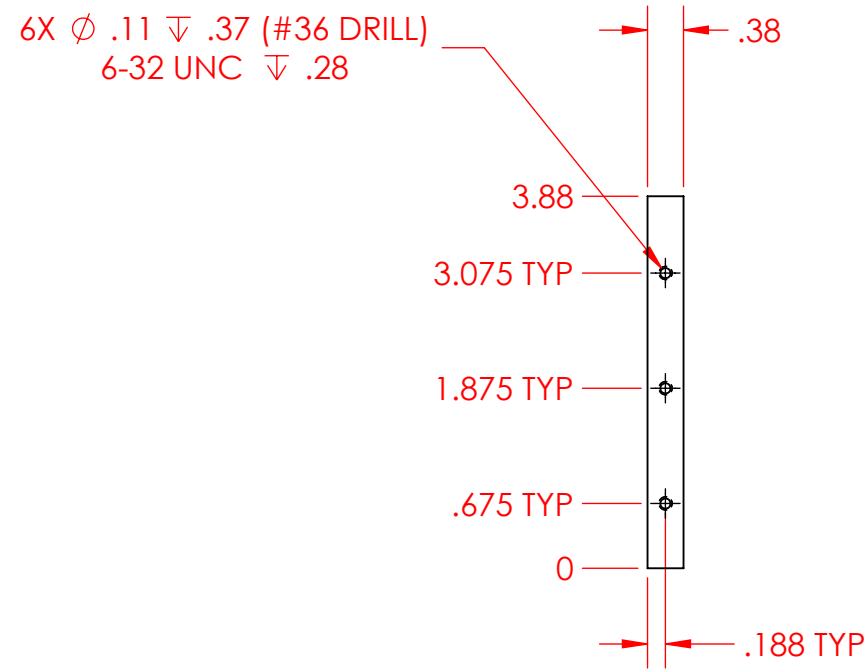
4

3

2

1

- NOTES:
- BOM ITEM 13: BOWDEN TERMINATION PLATE PLATE
 - MATERIAL: Al 6061



<p>PROPRIETARY AND CONFIDENTIAL</p> <p>THE INFORMATION CONTAINED IN THIS DRAWING IS THE SOLE PROPERTY OF VA PUGET SOUND RR&D CENTER FOR LIMB LOSS AND MOBILITY (CLIMB). ANY REPRODUCTION IN PART OR AS A WHOLE WITHOUT THE WRITTEN PERMISSION OF CLIMB IS PROHIBITED.</p>	UNLESS OTHERWISE SPECIFIED:		 <p>Center for Limb Loss and MoBility</p>		TITLE:			
	<p>DIMENSIONS ARE IN INCHES</p> <p>TOLERANCES:</p> <p>TWO PLACE DECIMAL \pm 0.005</p> <p>THREE PLACE DECIMAL \pm 0.003</p>				<p>KNEE BRACE MOTOR CHASSIS</p>			
	INSPECT CRITICAL DIMENSIONS, SEE SHEET 1	INTERPRET GD&T PER:	ASME Y14.1-2009	NAME	DATE	SIZE	DWG. NO.	REV
MATERIAL SPECIFIED IN NOTES OF EACH SHEET	DO NOT SCALE DRAWING	CHECKED	DRAWN	D. REINSDORF	1 OCT 18	B		2.2
SEE SHEET 1 FOR REVISION HISTORY						SCALE: 1:2	WEIGHT:	SHEET 5 OF 7

4

3

2

1

B

B

A

A

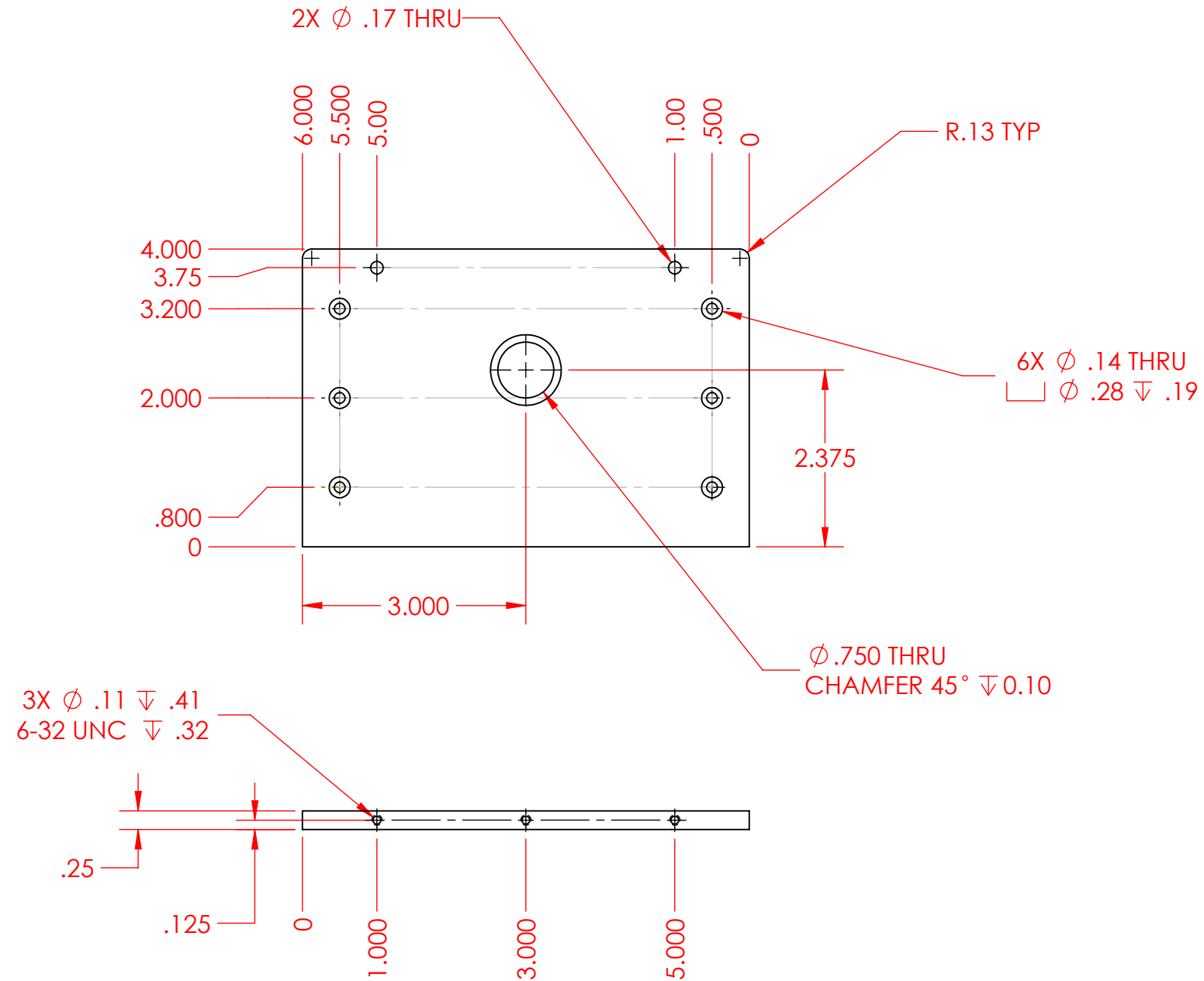
4

3

2

1

- NOTES:
- BOM ITEM 4: BASE PLATE
 - MATERIAL: Al 6061



<p>PROPRIETARY AND CONFIDENTIAL</p> <p>THE INFORMATION CONTAINED IN THIS DRAWING IS THE SOLE PROPERTY OF VA PUGET SOUND RR&D CENTER FOR LIMB LOSS AND MOBILITY (CLIMB). ANY REPRODUCTION IN PART OR AS A WHOLE WITHOUT THE WRITTEN PERMISSION OF CLIMB IS PROHIBITED.</p>	<p>UNLESS OTHERWISE SPECIFIED:</p> <p>DIMENSIONS ARE IN INCHES</p> <p>TOLERANCES:</p> <p>TWO PLACE DECIMAL \pm 0.005</p> <p>THREE PLACE DECIMAL \pm 0.003</p>	 <p>Center for Limb Loss and MoBility</p>	<p>TITLE:</p> <p>KNEE BRACE MOTOR CHASSIS</p>														
	<p>INSPECT CRITICAL DIMENSIONS, SEE SHEET 1</p> <p>MATERIAL SPECIFIED IN NOTES OF EACH SHEET</p> <p>SEE SHEET 1 FOR REVISION HISTORY</p>		<p>INTERPRET GD&T PER:</p> <p>ASME Y14.1-2009</p> <p>DO NOT SCALE DRAWING</p>	<table border="1"> <tr> <td>NAME</td> <td>DATE</td> </tr> <tr> <td>DRAWN D. REINSDORF</td> <td>1 OCT 18</td> </tr> <tr> <td>CHECKED</td> <td></td> </tr> </table>	NAME	DATE	DRAWN D. REINSDORF	1 OCT 18	CHECKED		<table border="1"> <tr> <td>SIZE</td> <td>DWG. NO.</td> <td>REV</td> </tr> <tr> <td>B</td> <td></td> <td>2.2</td> </tr> </table>	SIZE	DWG. NO.	REV	B		2.2
NAME	DATE																
DRAWN D. REINSDORF	1 OCT 18																
CHECKED																	
SIZE	DWG. NO.	REV															
B		2.2															

4

3

2

1

B

B

A

A

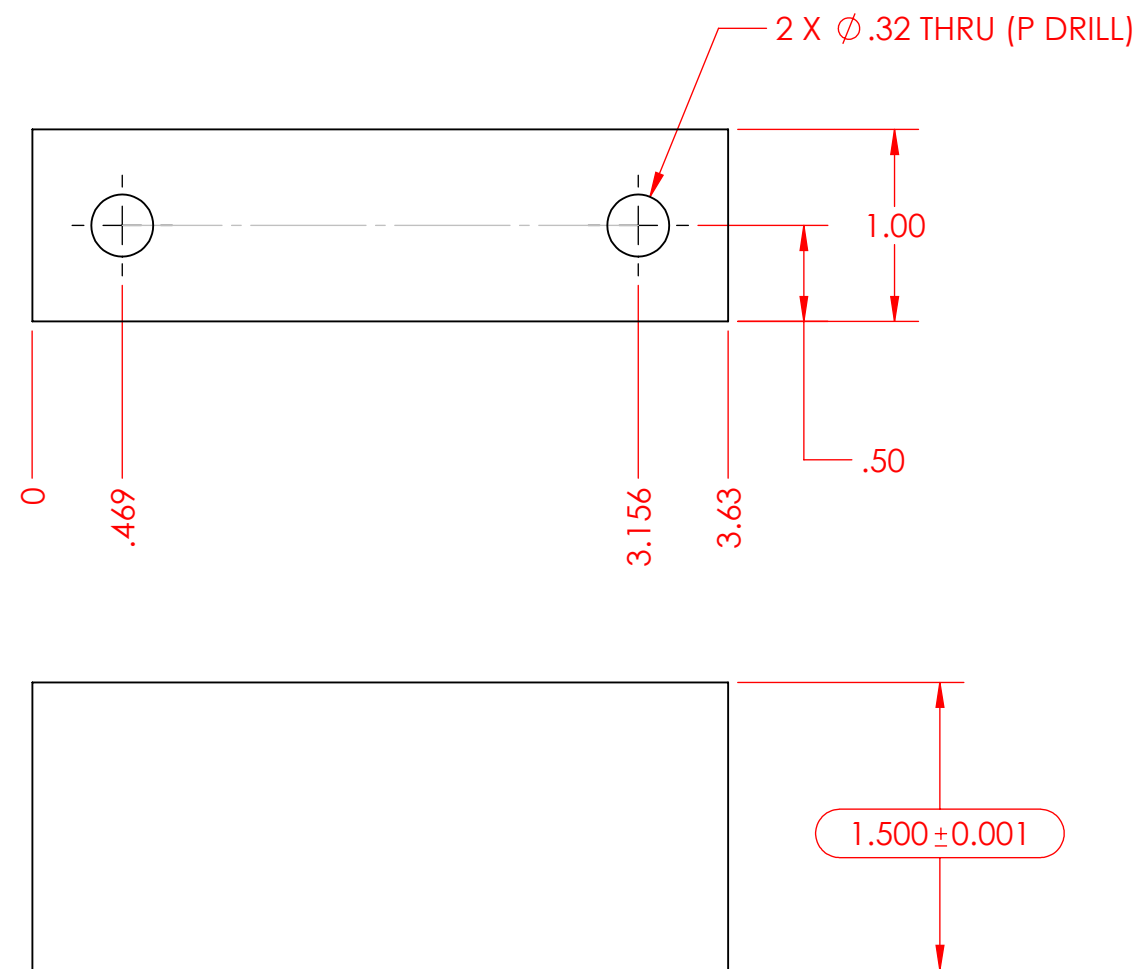
4

3

2

1

- NOTES:
- BOM ITEM 8: BEARING MOUNT PLATE
 - MATERIAL: AI 6061



PROPRIETARY AND CONFIDENTIAL THE INFORMATION CONTAINED IN THIS DRAWING IS THE SOLE PROPERTY OF VA PUGET SOUND RR&D CENTER FOR LIMB LOSS AND MOBILITY (CLIMB). ANY REPRODUCTION IN PART OR AS A WHOLE WITHOUT THE WRITTEN PERMISSION OF CLIMB IS PROHIBITED.	UNLESS OTHERWISE SPECIFIED: DIMENSIONS ARE IN INCHES TOLERANCES: TWO PLACE DECIMAL ± 0.005 THREE PLACE DECIMAL ± 0.003	 Center for Limb Loss and MoBility	TITLE: KNEE BRACE MOTOR CHASSIS			
	INSPECT CRITICAL DIMENSIONS, SEE SHEET 1 MATERIAL SPECIFIED IN NOTES OF EACH SHEET SEE SHEET 1 FOR REVISION HISTORY		INTERPRET GD&T PER: ASME Y14.1-2009 DO NOT SCALE DRAWING	NAME D. REINSDORF	DATE 1 OCT 18	SIZE B
			SCALE: 1:2	WEIGHT:	SHEET 7 OF 7	

4

3

2

1

B

B

A

A

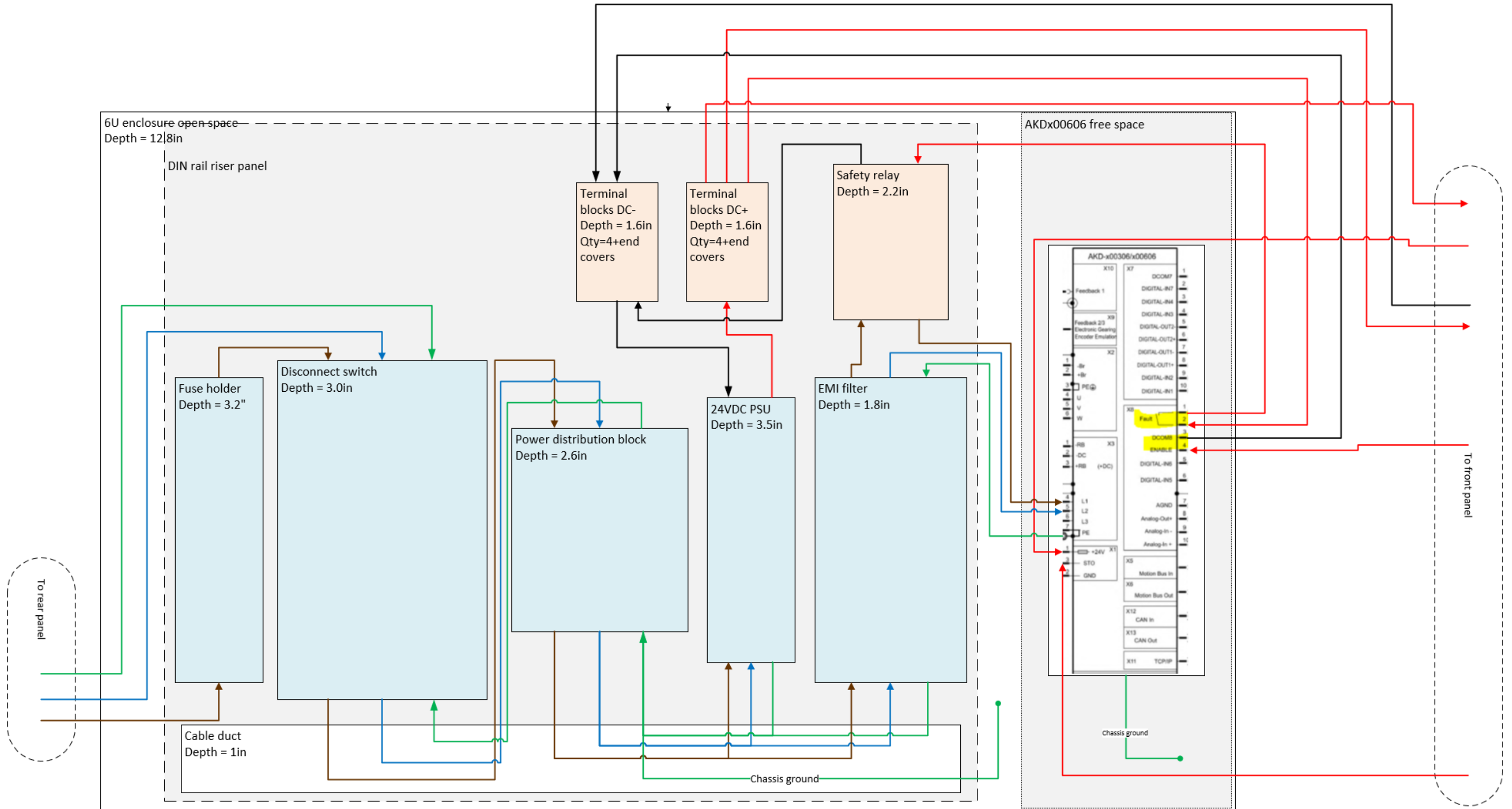
ABLE Motor Transmission BOM

Description	Manufacturer or supplier	P/N	Qty	Notes
Motor	Kollmorgen	AKM52H-ANDNCA00	1	
Bowden conduit	Lexco	B415218-00-01	N/A	Length/qty setup dependent
Bowden rope	West Marine	16901779	N/A	
Bowden adjusters	Lexco	21-1064-76M	2	Qty of 1 required for knee brace, 1 for motor chassis
Bowden adjuster nuts (1/4-28)	McMaster Carr	91847A429	4	
Motor mount plate	Approved machine shop	9057K24	1	McMaster stock P/N listed, see CAD files for GD&T
Bearing mount plate	Approved machine shop	9057K14	1	
Shear wall plate	Approved machine shop	9057K182	1	
Base plate	Approved machine shop	9057K181	1	
Bearing riser	Approved machine shop	9057K446	2	
Bowden termination plate	Approved machine shop	9057K222	1	
5/8" D-profile shaft SS303	McMaster Carr	8632T147	1	
Mounted bearing	FYH Bearing units USA	2353K31/UCPP202-10S6H1	1	
Shaft coupling	Zero-Max	SC060R 0.500 NKW X 24MM K6 SIDE NKW	1	
Foot	McMaster Carr	9306K821	4	
Handle	McMaster Carr	5245A6	2	
10-32 screw, motor plate	McMaster Carr	92196A269	2	
M8 screw for motor	McMaster Carr	91292A145	4	
M8 nut for motor	McMaster Carr	93033A102	4	
8-32 screw, handle	McMaster Carr	92949A193	4	
6-32 screw	McMaster Carr	9219A146	15	
1/4-20 screw, feet	McMaster Carr	92196A534	4	
6-32 heat set insert, cable sheave	McMaster Carr	93365A130	1	
6-32 set screw, cable sheave	McMaster Carr	92311A142	1	

APPENDIX C: MOTOR DRIVE POWER CIRCUIT DESIGN

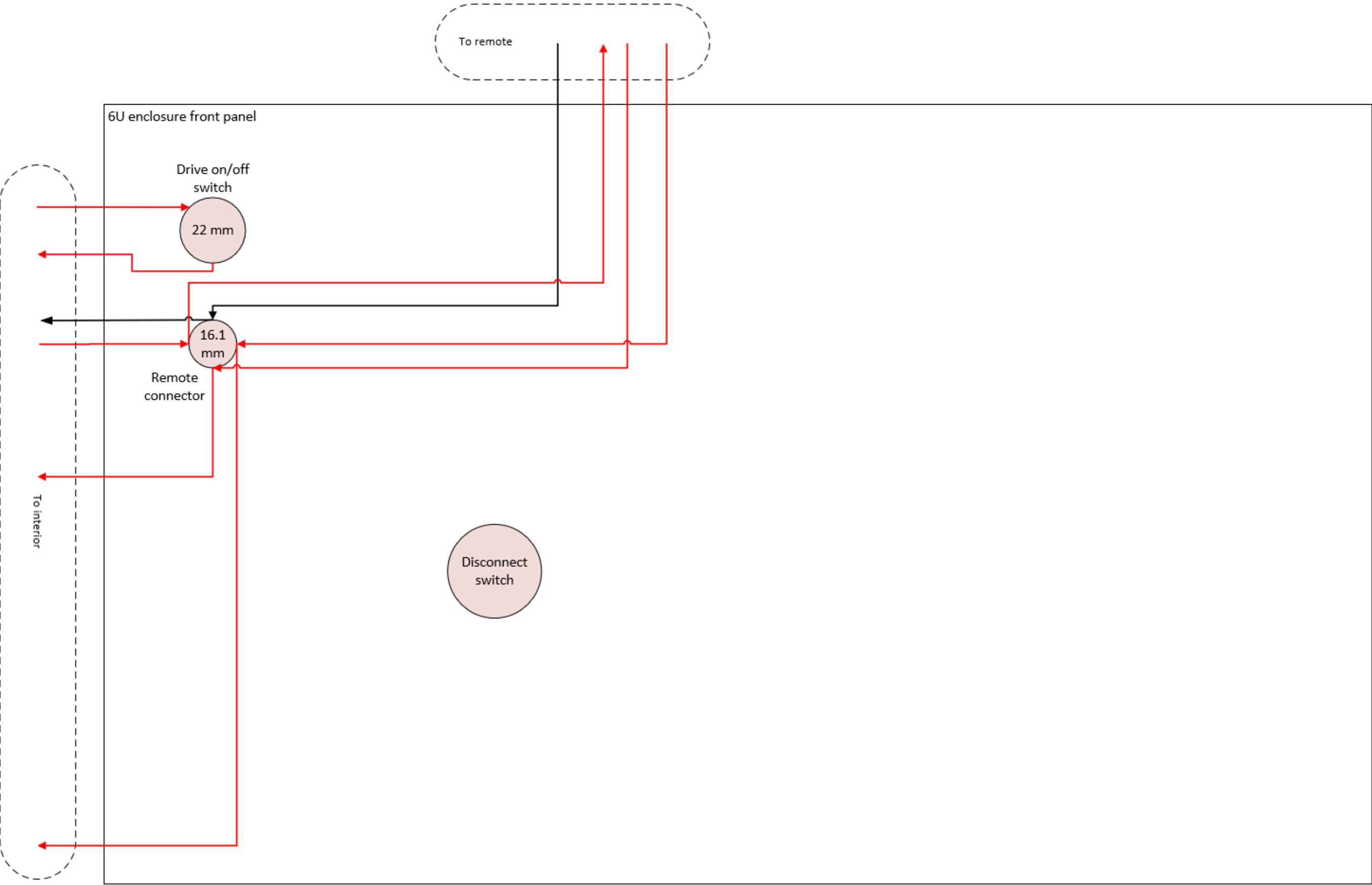
Drive power electronics wiring diagram

Enclosure interior



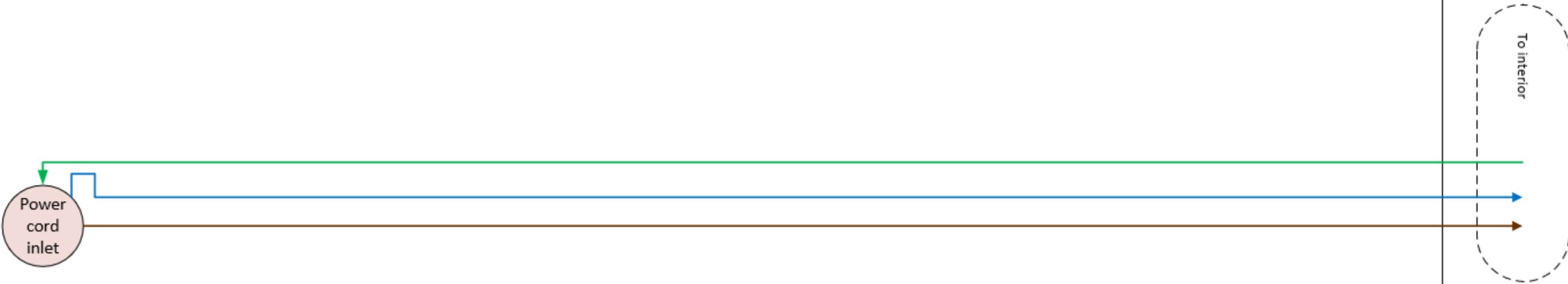
Drive power electronics wiring diagram

Enclosure front panel

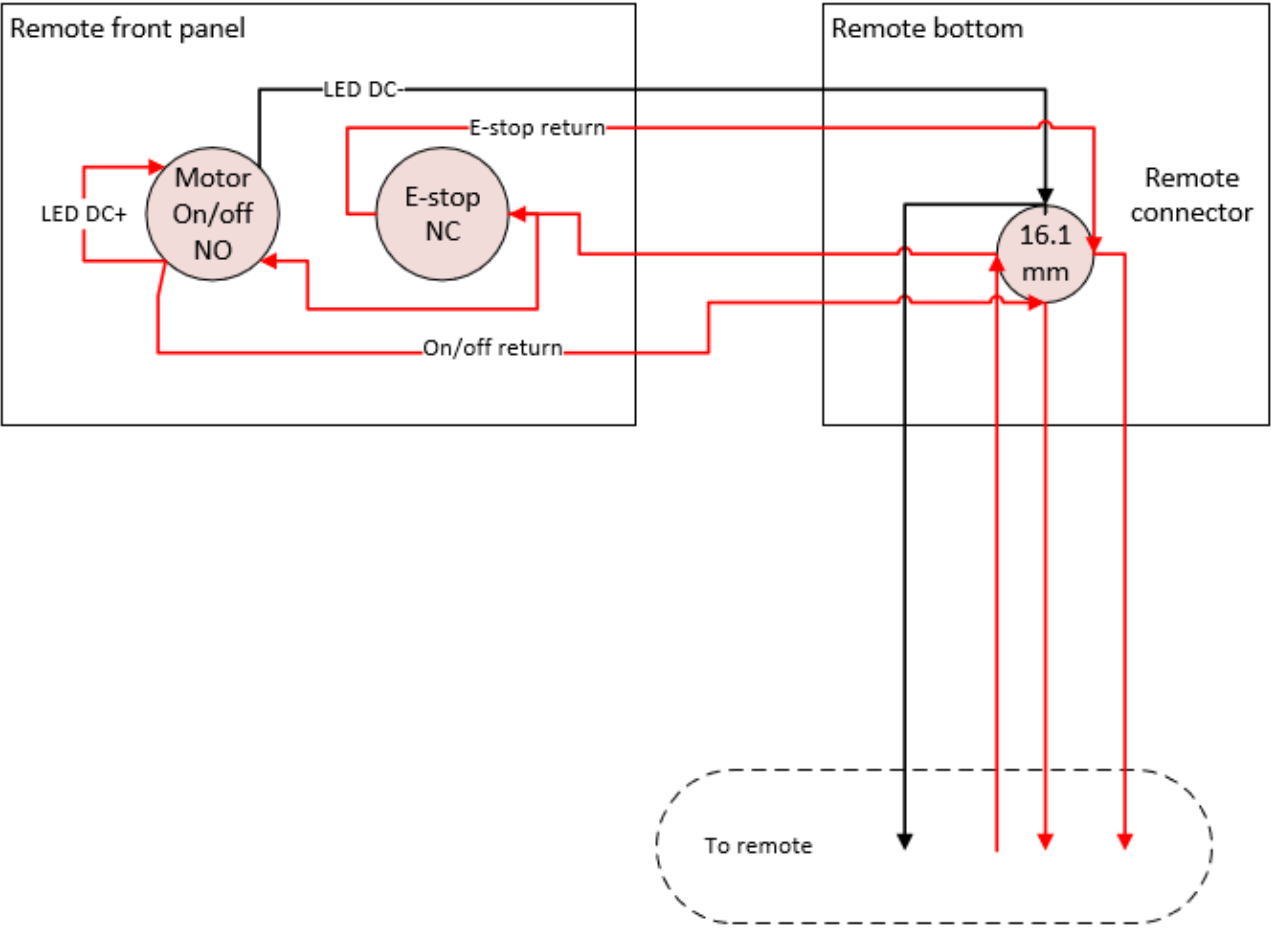


Enclosure rear panel

6U enclosure rear panel



Remote



ABLE Drive Power Electronics and Enclosure BOM

Actuation

Description	Manufacturer or supplier	P/N	Qty	Notes
Motor cable	Kollmorgen	CCJ1A2-015-006-00	1	
Drive	Kollmorgen	AKD-P00606-NBEC-0000	1	

Power components

Description	Manufacturer or supplier	P/N	Qty	Notes
Mains filter	Eaton	ADPV12005		
Contactora	Socomec	22013003	1	
Contactora shaft	Socomec	14070532	1	
Contactora handle - external mount	Socomec	14841111	1	
Contactora handle - direct mount	Socomec	22995032	1	
24VDC PSU for logic circuit	RHINO	PSB24-060-P	1	
15A fuse	Edison	JHL15-1	1	
Fuse holder	McMaster Carr	7721K16	1	
EMI input filter	Roxburgh	RES90F16	1	
Spade connectors for EMI filter	McMaster Carr	72625K77	4	
Safety relay for motor disconnect	Lovato	BF1210D024	1	Drive disconnects motor when fault triggered
Power distribution block for AC	McMaster Carr	6367T19		
Terminal blocks for DC logic, red and black	McMaster Carr	7641K921	3	Qty is per color
Terminal block end stop	McMaster Carr	7641K35	3	Qty is for both DC+ and DC- blocks
Terminal block end cover	McMaster Carr	7641K33	2	Qty is for both DC+ and DC- blocks
Terminal block jumper	McMaster Carr	7641K925	2	Qty is in sets of jumpers
Cord grip for power cable enclosure exit	McMaster Carr	69915K63		

ABLE Drive Power Electronics and Enclosure BOM

Remote

Description	Manufacturer or supplier	P/N	Qty	Notes
Motor on/off switch	Fuji electric	AR22F5L-10E3GZA	1	
Motor legend plate	Eaton	E22NS81	1	
E-stop switch	Eaton	E22LTA2QB	1	
E-stop legend plate	Eaton	ECX1651	1	
Enclosure	Automation direct	SA106-40SL	1	
Male M12 bulkhead connector	Automation direct	7231-13501-9710050	1	
M12 cable male to female, 9.8ft	Automation direct	7000-40021-0240300	1	

Enclosure

Description	Manufacturer or supplier	P/N	Qty	Notes
6U DIN rail rackmount enclosure	Hammond Manufacturing	RMCV191013BK1	1	
Drive on/off switch	Fuji electric	AR22WR-210BZA	1	
Drive on/off switch legend plate	Eaton	E22NS42	1	
Cable for drive on/off switch to front panel	Automation direct	7000-08081-0200200	1	Allows for quick disconnect of front panel from enclosure
Male M8 bulkhead connector to drive on/off switch	Automation direct	7000-08553-9700050	1	Mounted behind front panel. Allows for quick disconnect of front panel from enclosure
Cable for remote connection to front panel	Automation direct	7000-12341-0240200	1	Allows for quick disconnect of front panel from enclosure
Male M12 bulkhead connector for remote connection to front panel	Automation direct	7231-13501-9710050	1	Mounted inside front panel. Allows for quick disconnect of front panel from enclosure
Female M12 bulkhead connector for remote connection to front panel	Automation direct	7231-13541-9710050	1	Mounted outside front panel. Allows for quick disconnect of remote from enclosure
Hook and loop cable tie for motor cable	McMaster Carr	6605K91	1	For cable management
Hook and loop cable tie for power cable	McMaster Carr	6605K92	1	For cable management

ABLE Drive Power Electronics and Enclosure BOM

Enclosure (cont)

Description	Manufacturer or supplier	P/N	Qty	Notes
Expandable push-in grommet for ethernet cable through front panel	McMaster Carr	4946A2	1	For cable management
Cord grip for power cord	McMaster Carr	69915K67	1	For cable management
Adhesive-back cable holder	McMaster Carr	7565K46	2	For cable management inside panel
1/4"x10"x12" Al 6061 for shelf	McMaster Carr	8975K561	1	To raise all components minus drive off back of enclosure, closer to front
Corner bracket to secure shelf at end	McMaster Carr	47065T833	2	Without bracket shelf would be cantilevered and only supported by back of enclosure
Standoff for raised DIN panel, 6" long	McMaster Carr	91780A210	5	Raised internal panel for DIN rail to ease component access
Standoff for raised DIN panel, 1.5" long	McMaster Carr	93505A199	5	Raised internal panel for DIN rail to ease component access
Washer for raised DIN panel, 1/4	McMaster Carr	92141A029	5	Raised internal panel for DIN rail to ease component access
Lock washer for raised DIN panel, 1/4	McMaster Carr	92146A029	5	Raised internal panel for DIN rail to ease component access
Thumb screw for front panel	McMaster Carr	91185A257	4	

ABLE Drive Power Electronics and Enclosure BOM

Wiring

Description	Manufacturer	P/N	Qty	Notes
Shielded wire (filter to drive)	McMaster	6452T26	2ft	
12 gauge wire for AC, green, blue, brown	McMaster	9874T14		
Power cable wire, 12 gauge, 10ft	McMaster	7082K24	1	
Power cable blade connector NEMA 5-15	McMaster	7196K31	1	
Grounding wire for drive to chassis, 6" long	McMaster	2196K41	1	
Grounding wire for PE to chassis, 11" long	McMaster	2196K42	1	
22 gauge wire for DC, black, red	McMaster	8251T2		
Pin terminals for DC to safety relay connection	McMaster	8009K15	2	Relay close to top of enclosure, bent to 90deg and used for clearance
Pin terminals for AC to safety relay connection	McMaster	8009K16	2	Relay close to top of enclosure, bent to 90deg and used for clearance
#10 ring terminal for protective earth connection	McMaster	7113K12	2	
1/4" ring terminal for protective earth connection	McMaster	7113K13	3	
1/4" external tooth washer for PE to enclosure	McMaster	95584A207	2	

**APPENDIX D: CODE AND EXAMPLE RESULT FOR
TRAJECTORY GENERATION**

Contents

- [Input](#)
- [Output](#)

```
% Dylan Reinsdorf
% Rev 1.0

% PURPOSE
% Calling script for trajectory generation function to test performance.

clc, clear all, close all
```

Input

```
yrange = [1 8.1]; % min and max y values
xt = [0.05 0.15; 0.6 0.8]; % transition values in x for rising/loading and falling/unloading
sections of profile
samples = 1000; % discretized sample qty
mode = 1; % numerical routine mode

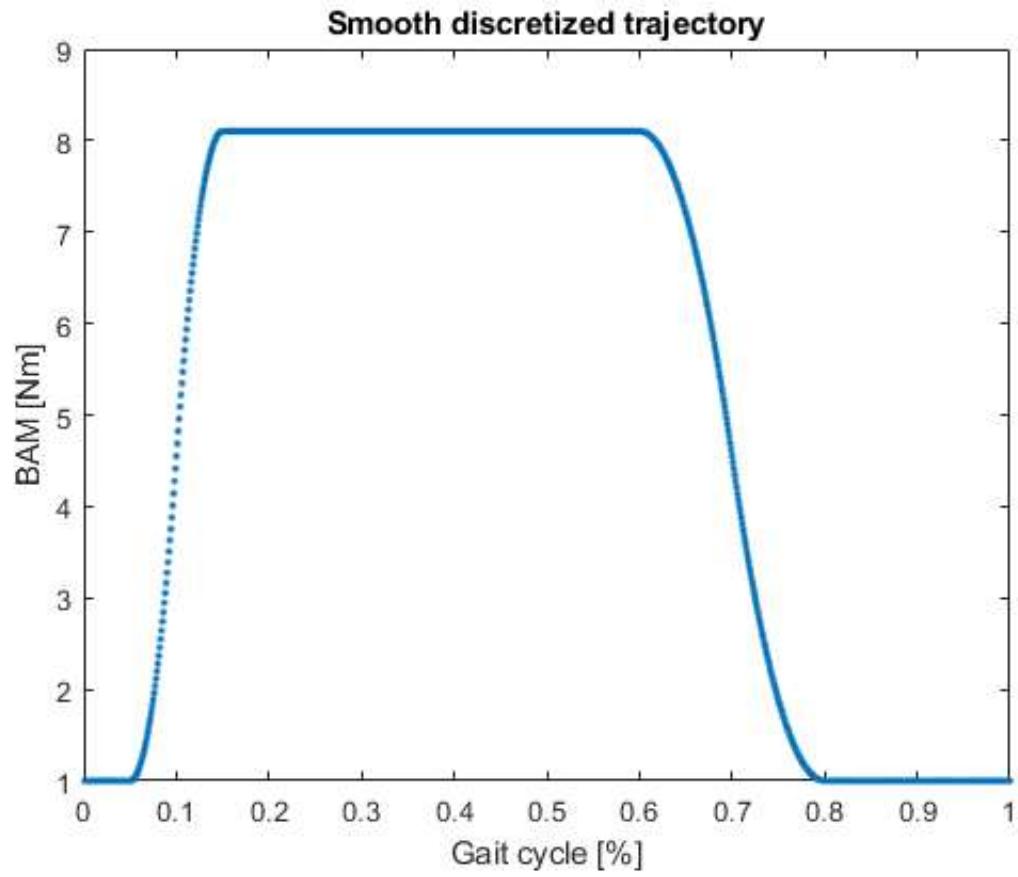
% the following is not currently in use, but should be added
% Define accel limit
% The max acceleration is defined as (dependent var)/time^2, in this case
% force/sec^2. As the trajectory is computed over a normalized gait cycle
% from 0 to 1, a worst case (fastest) pace is assumed and used to compute
% an accel limit in lbf/gc^2, which agrees with the base unit system used
% to compute the trajectory in the subsequent section.
pacemax = 1.5; % max gait cycles (gc) per second [gc/s]
amax = 1500; % max acceleration [lbf/s^2]
alim = amax*(1/pacemax)^2;
alim = 10000;
```

Output

```
% Run trajectory generator
[X,Y, pass] = KBtraj(yrange, xt, samples, alim, mode);

% Tasks to perform based on whether a solution was ('pass=1') or was not ('pass=0') found
if min(pass) > 0 % solution found
    % plot
    figure(1)
    plot(X,Y, '.')
    xlabel('Gait cycle [%]')
    ylabel('BAM [Nm]')
    title('Smooth discretized trajectory')
else % solution not found
    disp('The specified trajectory cannot be carried out with the specified parameters')
    disp('Suggestions: increase the acceleration x interval, change the max acceleration, or
    change the target forces')
    disp('You may also add an element to itol, with an increased value, e.g. if the largest
    element in itol = 4, then add an element with magnitude = 6')
```

end



Contents

- [Declare inputs](#)
- [Solve numerically](#)

```
function [X,Y, pass] = KBtraj(yrange, xt, samples, alim, mode)
```

```
% Dylan Reinsdorf
% Rev 1.0

% PURPOSE
% This function parameterizes and computes a normalized trajectory intended
% for the active unloader KOA brace. It serves as the top level function
% for calling child functions that compute sections of the full trajectory
% profile. See Description for additional details.

% DESCRIPTION
% Profile is found as five separate sections, the full profile is output as
% the five sections concatenated. The sections are:
% (1) ymin, order 0
% (2) rise, order 2
% (3) ymax, order 0
% (4) fall, order 2
% (5) ymin, order 0

% INPUTS
% - alim: acceleration limit with IV of gait cycles
% - mode: numerical routine mode, see child function file for details
% - samples: qty of discretized samples

% To do
% - change isreal check
% - is isreal required?
```

Declare inputs

Cast inputs into form used for trajectory parameterization/computation

```
ymin = yrange(1);
ymax = yrange(2);
dx = 1/samples; % discretization in x
```

Solve numerically

Find rising and falling sections of profile

```
[X2,Y2,pass2] = accelsmooth(xt(1,1),xt(1,2), ymin, ymax, dx, alim, mode); % rising section
[X4,Y4,pass4] = accelsmooth(xt(2,1),xt(2,2), ymin, ymax, dx, alim, mode); % falling section
% reverse falling section order since accelsmooth computes it as a rising
% section
```

```
Y4 = fliplr(Y4);

% Create constant (zero order) sections for (1) ymin, (3) ymax, (5) ymin
[X1,Y1] = zeroOrdrPrfl(ymin, dx, xt(1,1)-dx, dx);
[X3,Y3] = firstOrdrPrfl(Y2(end), Y4(1), xt(1,2)+dx, xt(2,1)-dx, dx);
[X5,Y5] = zeroOrdrPrfl(ymin, xt(2,2)+dx, 1, dx);

% Concatenate result
X = [X1, X2, X3, X4, X5];
Y = [Y1, Y2, Y3, Y4, Y5];
pass = [pass2, pass4];
```

```
end
```

Contents

- [Declare inputs](#)
- [Define loop conditions/parameters](#)
- [Find](#)

```
function [X,Y, pass] = accelsmooth(xa0,xaf, ya0, yaf, dx, alim, mode)
```

```
% Dylan Reinsdorf
% Rev 1.0

% PURPOSE
% Find an acceleration profile numerically. The profile starts at (xa0,
% Fmin) and ends at (xaf, Fmax). The function connects these endpoints via
% a smooth profile that meets the force tolerance 'Ftol' and
% acceleration limit 'alim' constraints.

% DESCRIPTION
% The generated profile is a combination of a C2 (2nd derivative continuous)
% and C1 (1st derivative continuous). The first C2 portion begins at (xa0,
% Fmin) and the second ends at (xaf, Fmax), the C1 portion connects the C2
% portions. The first C2 portion is concave up, the second is concave down.
%
% To simplify computation, this function:
% (1) finds the three portions relative to (0,0), i.e. the element 1 of the
% first C2 portion is at (0,0). This simplifies computation.
% (2) concatenates the three portions to get a single discretized profile.
% (3) shifts the full profile origin to the desired location @ (xa0, Fmin).

% INPUTS
% - mode: the operation mode of the numerical routine, it can favor either
% computation time or minimal acceleration
% - mode == 0: favor computation time, the routine takes large 'steps'
% that will likely find a solution that meets the input constraints using
% a non-minimal acceleration
% - mode == 1: favor acceleration minimization, finds acceleration
% that meets the input constraints using small 'steps' therefore taking
% more computation time, but yielding a profile with smaller
% accelerations than mode == 0.

% To do
% DEFINE THE CONSTRAINTS
% DEFINE INPUTS
% Document how tolerancing is used and looping, how approach favors speed,
% and how to change it to favor minimum acceleration (change da to fixed
% step sizes)
```

Declare inputs

```
% Cast boundary conditions into space used to compute acceleration profile
x0 = xa0;
```

```

y0 = ya0;
yf = (yaf-ya0)/2;
xf = (xaf-xa0)/2;

% Force tolerance
% the tolerance band that all max min force values ('Fmax', 'Fmin') must
% lie within for the computed trajectory
Ftol = 0.01; % e.g. a value of 0.1 corresponds to +- 10% force [% force]

```

Define loop conditions/parameters

```

% Find seed value for numerical procedure
% the numerical procedure iterates through acceleration values, starting at
% the lowest that yields a real valued solution, then increases the
% acceleration until one is found that satisfies constraints
a0 = ceil(yf/xf^2); % initial acceleration
if alim<a0 % if true, then a real valued accel !exist that meets the input acceleration limit
    requirement, therefore break
    disp('The specified trajectory cannot be carried out within the acceleration limit')
    disp([xa0,xaf])
    disp([ya0,yaf])
    disp(a0)
    return
end

% declare outer while loop parameters
itol = [1 2 3 4];
i1 = 0; % selects tolerance elements from 'itol' in the while loop below
pass = 0; % variable to track whether a solution was found

```

Find

```

while i1 < length(itol)
    i1 = i1 + 1; % increment i1

    % declare inner while loop inputs
    a = a0;
    loop = 1;

    % select routine operation mode
    if mode == 0
        da = (alim-a0)/(10^itol(i1)); % acceleration step size
    elseif mode ==1
        da = 1/(10^(itol(i1)));
    else
        disp('Operation mode input required')
        return
    end

    while loop == 1
        xm = (a*xf - ((a*xf)^2 - a*yf)^(1/2))/a;
        % eval constraints
        creal = isreal(xm); % test if real
    end
end

```

```

        cint = round(xm/dx,itol(i1)) == round(xm/dx); % test if xm falls near the dx spacing
of the range xf-x0
        if creal && cint == 1
            loop = 0;
        end
        a = a + da;
        if a > alim % stop looping if the accel limit is reached and advance to next outer while loop cycle
            loop = -1;
        end
    end
end

if loop == 0 % if solution found from above while loop then discretize trajectory

% find new xm - the xm found above may not be exactly on the interval dx
% (but it's close), which results in a discontinuity at x = xm. Therefore, find
% the xm that is exactly on the interval. Note that this results in the
% value Fmax not being reached exactly, this will be checked below
xm = round(xm/dx)*dx;

% Discretize trajectory
X1 = 0:dx:xm-dx; % const accel section input vector
X2 = xm:dx:2*xf-xm; % const vel section input vector
f1 = a*X1.^2; % const accel output
f2 = 2*a*xm*(X2-xm)+a*xm.^2; % const vel output

% Create decelerating section
% performed by mirroring f1 over x and y dirs, then shifting vertically
f3 = -f1; % flip over x dir
f3 = fliplr(f3); % flip over y dir
vshift = f2(end)+f2(1)-f1(end)-f3(1); % required vertical shift
f3 = f3+vshift; % shift vertically

% Append results to yield full discretized accel profile
X = 0:dx:xf*2;
Y = [f1, f2, f3];

% if the final force is within the tolerance band then stop loop
% execution, else continue to next outer while loop iteration
if 2*yf*(1-Ftol) <= f3(end) && f3(end) <= 2*yf*(1+Ftol)
    pass = 1; % solution found
    % shift input and output back to origin
    X = X + x0;
    Y = Y + y0;
    break
end

end % end discretization step
end % end outer while

end % end function

```

```
function [X,Y] = firstOrdrPrfl(y0, yf, x0, xf, dx)
% Dylan Reinsdorf
% Rev 1.0

% PURPOSE
% Generate a discretized first order profile subject to scalar boundary
% condition inputs x0, xf, y0, yf at spacing dx.

X = x0:dx:xf;
m = (yf-y0)/(xf-x0);
Y = m*X+y0;
end
```

```
function [X,Y] = zeroOrdrPrfl(y, x0, xf, dx)
% Dylan Reinsdorf
% Rev 1.0

% PURPOSE
% Generate a discretized zero order profile subject to scalar boundary
% condition inputs x0, xf, y at spacing dx.

X = x0:dx:xf;
Y = ones(1,length(X))*y;
end
```